Mon. Not. R. Astron. Soc. **372,** 1259–1274 (2006) doi:10.1111/j.1365-2966.2006.10925.x

Ages, metallicities and [α/Fe] ratios of globular clusters in NGC 147, 185 and 205

M. E. Sharina,[1⋆] V. L. Afanasiev[1⋆] and T. H. Puzia[2⋆]

[1]*Special Astrophysical Observatory, Russian Academy of Sciences, N. Arkhyz, KChR, 369167, Russia*
[2]*Space Telescope Science Institute, 3700 San Martin Drive, Baltimore, MD 21218, USA*

Accepted 2006 August 10. Received 2006 August 7; in original form 2006 March 31

ABSTRACT

We present measurements of ages, metallicities and [α/Fe] ratios for 16 globular clusters (GCs) in NGC 147, 185 and 205 and of the central regions of the diffuse galaxy light in NGC 185 and 205. Our results are based on spectra obtained with the SCORPIO multislit spectrograph at the 6-m telescope of the Russian Academy of Sciences. We include in our analysis high-quality *Hubble Space Telescope*/WFPC2 photometry of individual stars in the studied GCs to investigate the influence of their horizontal branch (HB) morphology on the spectroscopic analysis. All our sample GCs appear to be old ($T > 8$ Gyr) and metal-poor ([Z/H] $\lesssim -1.1$), except for the GCs Hubble V in NGC 205 ($T = 1.2 \pm 0.6$ Gyr, [Z/H] $= -0.6 \pm 0.2$), Hubble VI in NGC 205 ($T = 4 \pm 2$ Gyr, [Z/H] $= -0.8 \pm 0.2$) and FJJVII in NGC 185 ($T = 7 \pm 3$ Gyr, [Z/H] $= -0.8 \pm 0.2$). The majority of our GCs sample has solar [α/Fe] enhancement in contrast to the halo population of GCs in M31 and the Milky Way. The HB morphologies for our sample GCs follow the same behaviour with metallicity as younger halo Galactic GCs. We show that it is unlikely that they bias our spectroscopic age estimates based on Balmer absorption-line indices. Spectroscopic ages and metallicities of the central regions in NGC 205 and 185 coincide with those obtained from colour–magnitude diagrams. The central field stellar populations in these galaxies have approximately the same age as their most central GCs (Hubble V in NGC 205 and FJJIII in NGC 185), but are more metal-rich than the central GCs.

Key words: globular clusters: general – galaxies: abundances – galaxies: individual: NGC 147 – galaxies: individual: NGC 185 – galaxies: individual: NGC 205 – galaxies: star clusters.

1 INTRODUCTION

Understanding the role of dwarf galaxies and their globular cluster systems (GCS) as building blocks of massive early-type and spiral galaxies is one of the great challenges of modern astrophysics. Studying the chemical compositions and colour–magnitude diagrams (CMDs) of globular clusters (GCs) in the nearby low-mass galaxies is critical to compare properties of these long-living objects situated in galaxies of different type and mass. Only the Local Group (LG) dwarf galaxies are close enough so that their GCs can be resolved into single red giant and horizontal branch (HB) stars by today's observatories.

Three close companions of the Andromeda galaxy, NGC 147, 185 and 205, comprise the brightest end of the LG dwarf early-type galaxy luminosity function. The proximity to M31 in combination with the unusual properties of these three galaxies have attracted great attention of astronomers since the beginning of the twentieth century (we refer the reader to a monograph by Van den Bergh 2000 and a review by Mateo 1998 for details). NGC 205 and 185 are very unusual galaxies and do not resemble any galaxy within ∼10 Mpc. Both have a regular spheroidal shape and are composed mainly of old stars. At the same time, both galaxies have a considerable amount of gas, dust and a significant intermediate-age stellar component. These unique properties are most likely tightly related their unusual evolutionary histories (e.g. Davidge 1992; Lee, Freedman & Madore 1993; Young & Lo 1997; Butler & Martinez-Delgado 2005; Davidge 2005). Compared to its brighter cousins, NGC 147 is gas and dust free. Asymptotic giant branch (AGB) stars contribute only 2–3 per cent of the total light of this galaxy (Davidge 1994). By means of its stellar content, NGC 147 resembles a typical dwarf spheroidal galaxy in the LG. However, it is much more luminous. The distance to NGC 205, 185 and 147, their stellar populations and star formation histories are being studied actively (e.g. Butler & Martinez-Delgado 2005; Dolphin 2005; McConnachie et al. 2005). Table 1 summarizes their distances, brightnesses and reddenings used in this paper for the studied galaxies. We use a standard

⋆E-mail: sme@sao.ru (MES); vafan@sao.ru (VLA); tpuzia@stsci.edu (THP)

Table 1. Absolute magnitudes, distance moduli and reddenings from Schlegel, Finkbeiner & Davis (1998) used for the galaxies of our study [indices refer to 0: this work; 1: McConnachie et al. (2004)].

NGC	$M_{V,0}$	$(M-m)_0$	A_V
147	-15.1^1	23.95^1	0.580
185	-15.6^1	24.15^1	0.593
205	-16.2^0	24.38^0	0.206

reddening law with $A_V = 3.315\ E(B-V)$. We note that we find indications for a slightly smaller distance modulus, $(m-M)_0 = 24.38 \pm 0.1$ mag, for NGC 205 compared to the values derived by McConnachie et al. (2005), $(m-M)_0 = 24.58 \pm 0.07$ mag, and Dolphin (2005), $(m-M)_0 = 24.45 \pm 0.14$ mag, based on the results of our stellar photometry (see Section 3).

Each of our sample galaxies hosts a sizable GCS. The discovery of GCs in NGC 147, 185 and 205 includes the work of Hubble (1932), Baade (1944), Hodge (1974) and Ford, Jacoby & Jenner (1977, hereafter FJJ77) (see Da Costa & Mould 1988 and van den Bergh 2000 for details). All searches of GCs were carried out on photographic plates. The clusters were classified as being associated with the galaxies by their galactocentric radius. However, recent studies of GCSs in dwarf galaxies reveal GCs situated far from optical bodies of their host galaxies (see e.g. Hwang et al. 2005). It is likely that detailed wide-field investigations may discover additional GC candidates around NGC 147, 185 and 205 using new observational facilities and improved classification schemes which would allow the measurement of real physical sizes of the GCSs in these dwarf galaxies. Four extended GCs were discovered in the outer halo of M31 by Huxor et al. 2005) using INT-WFS images. Recent *Hubble Space Telescope* (*HST*) based surveys reveal new GC candidates in M31 (Barmby & Huchra 2001, see also the summary of optical and infrared photometry in Galleti et al. 2004). For instance, there are ∼50 objects in the catalogue of Galleti et al. (2004) within a radius of 20 arcmin around the centre of NGC 205. Galleti et al. (2006) emphasize that our knowledge about the M31 GCS is far from complete even in terms of simple membership and undertake a large spectroscopic survey of bona fide GCs and cluster candidates in M31. Obtaining radial velocities for GCs in the M31 halo and in the dwarf galaxies, detailed CMD and abundance studies will certainly help to solve the problem of the origin of M31 and of the satellite galaxies.

The properties of the GCs in NGC 147, 185 and 205 from the literature are summarized in Table 2. Da Costa & Mould (1988) first obtained spectra for eight Hubble clusters, the nucleus of NGC 205, FJJ77 clusters I–V in NGC 185 and for the two clusters Hodge I and III in NGC 147. A comparison of line strengths relative to similar spectra of Galactic GCs indicated that with a single exception, of the central GC Hubble V in NGC 205, all the clusters in NGC 147, 185 and 205 are old and metal-poor. The age estimates for Hubble V fall in a wide range from ∼300 Myr (based on *BVR* photometry, Lee 1996) to intermediate ages (based on *optical* and far-ultraviolet imaging with *HST*/WFPC2, Jones et al. 1996). Star cluster formation seems to be a more extended process in NGC 185. A star-forming region of Hα + [N II] emission with a diameter of 50 pc near the centre of NGC 185 may be a probable place of a massive young star cluster birth according to a modern evolutionary scheme (Gallagher & Grebel 2001 and references therein). Young & Lo (1997) estimated the mass of the brightest central H I clump in NGC 185 $M_{\rm H\,I} = 0.7 \times 10^4\ {\rm M}_\odot$ and the corresponding virial mass a factor of 100 higher. The clump is associated with a massive giant molecular cloud.

Table 2. Properties of GCs in NGC 147, 185 and 205 summarized from the literature. Columns contain the following data: (1) object name, (2) integrated V magnitude, (3) integrated $U-B$ colour, (4) integrated $B-V$ colour, (5) metallicity (indices refer to 1: Hodge (1974); 2: Hodge (1976); 3: Hodge (1973); 4: Da Costa and Mould (1988); 5: Geisler et al. (1999); 6: Butler & Martinez-Delgado (2005); 7: Sharov & Lyuty (1983); 0: our *HST*/WFPC2 integrated *VI* photometry corrected for Galactic extinction using Schlegel et al. (1998) maps. Asterisks indicate that $(V-I)_0$ colour is given instead of $(B-V)$.

Object	V	$U-B$	$B-V$	[Fe/H]
NGC 147				
Hodge I	17.7^2	0.6^2	0.8^2	-1.9^4
Hodge II	16.5^1	$0.4:^7$	0.6^7	–
Hodge III	17.0^2	0.1^2	0.6^2	-2.5^4
NGC 185				
FJJI	18.4^1	0.2^1	0.8^1	-1.4^4
FJJII	19.7^1	–	–	-1.2^4
FJJIII	16.8^1	0.1^1	0.9^1	$-1.7^4, -1.6^5$
FJJIV	19.0^4	0.05^1	0.7^1	$-2.5^4, -1.9^5$
FJJV	16.7^1	–	0.7^1	$-1.8^4, -1.5^5$
FJJVII	$18.9^{0,*}$	–	$1.0^{0,*}$	–
NGC 205				
Hubble I	16.9^3	–	0.8^3	-1.5^4
Hubble II	16.7^3	0.2^3	0.9^3	-1.5^4
Hubble V	16.7^3	$0.2:^3$	0.6^3	–
				–
Hubble VI	17.9^3	0.8^3	0.7^3	-1.3^4
Hubble VII	18.0^3	0.1^3	0.9^3	-1.4^4
Hubble VIII	16.6^3	0.1^3	0.7^3	-1.9^4

In this paper, we derive ages, metallicities and [α/Fe] ratios for GCs in NGC 147, 185 and 205 based on measurements of absorption-line indices as defined by the Lick standard system (Burstein et al. 1984; Worthey et al. 1994; Worthey & Ottaviani 1997; Trager et al. 1998). The main advantage of this system is its ability to disentangle age from metallicity using the information on the strength of prominent diagnostic absorption-line features measured in the intermediate-resolution integrated-light spectra.

The paper is organized as follows. In Section 2 we describe our spectroscopic data, the data reduction, as well as our methods and results of measuring Lick line indices in the spectra of GCs and the diffuse host galaxy light. In Section 3 we present results from our CMD photometry analysis of GCs, where we compare the loci of red giant branch (RGB) and HB stars with the Victoria-Regina stellar models of VandenBerg, Bergbusch & Dowler (2006). In Section 4 we discuss the derived evolutionary parameters for GCs and compare them with the data available in the literature.

2 SPECTROSCOPIC DATA

2.1 Observations and data reduction

The observations were performed with the multislit unit of the SCORPIO spectrograph (Afanasiev & Moiseev 2005), installed at the prime focus of the 6-m telescope of the *Russian Academy of Sciences*. Fig. 1 shows DSS-2-red images of NGC 147 and 185 with marked GCs as well as the 6-m telescope image of NGC 205 with

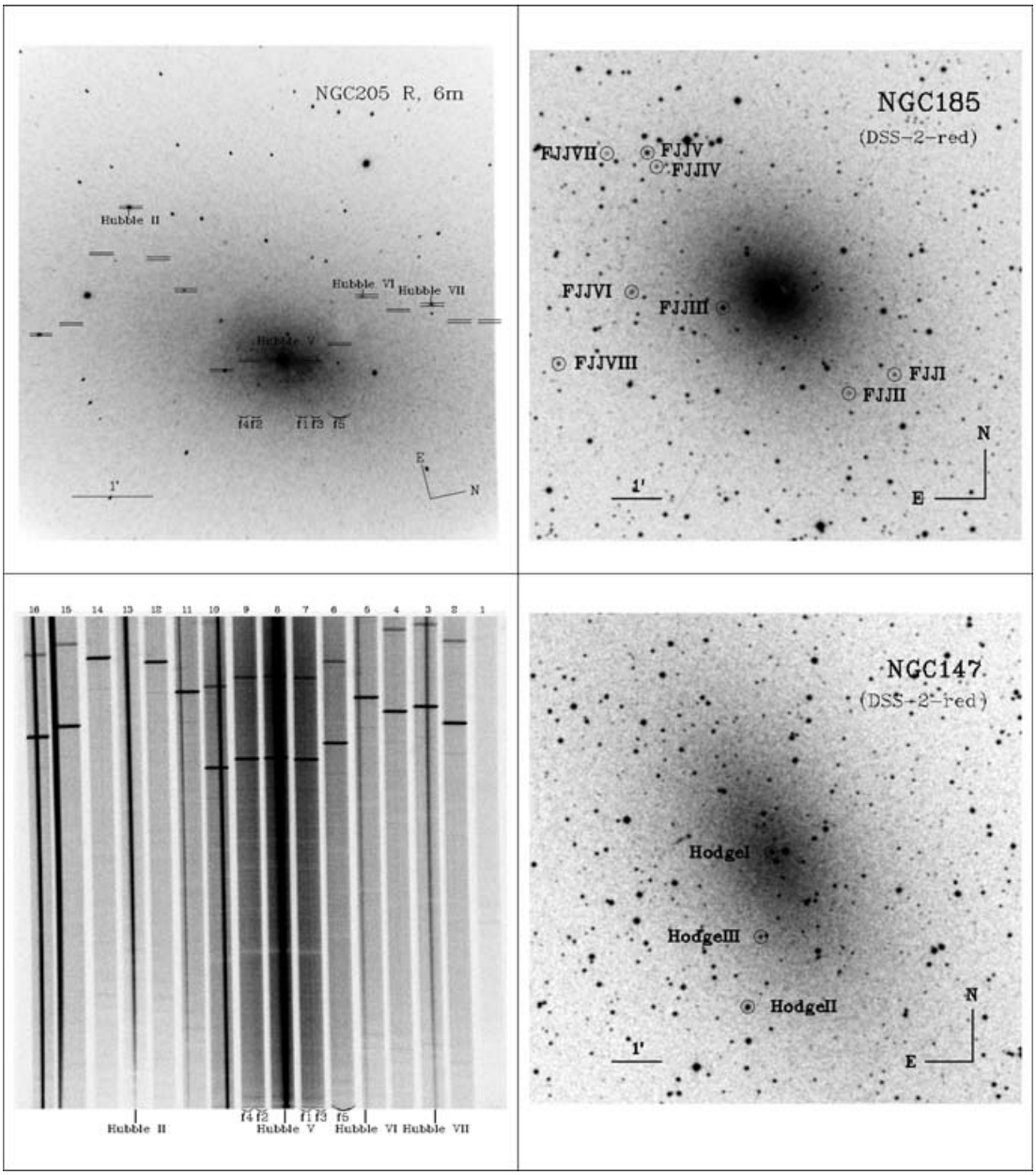

Figure 1. The upper left-hand panel shows an image of NGC 205 obtained with the SCORPIO multislit unit at the 6-m RAS telescope. Settings of slits on the GCs and diffuse galactic light regions are indicated. The lower left-hand panel shows a frame with raw non-reduced spectra of objects in NGC 205. Two right-hand panels show Digital Sky Survey 10 × 10-arcmin^2 images of NGC 185 and 147 with GCs.

marked settings of the slits and an image of the corresponding raw spectra. In multislit mode SCORPIO has 16 movable slits (1.2 × 18.0 arcsec^2) in the field of 2.9 × 5.9 arcmin^2 in the focal plane of the telescope. We use the CCD detector EEV42-40 with 2048 × 2048 pixel elements and the scale ∼0.18 arcsec pixel^{-1}. The grism GR1200g (1200 lines mm^{-1}) gives a spectral resolution ∼5 Å. The exact spectral coverage of an individual spectrum depends on the distance of the slit position from the meridian of the field. Most of our spectra have good wavelength coverage between 4200 and 5800 Å. Slit positions were set based on pre-imaging obtained with the same instrument.

A journal of observations is given in Table 3. GCs covered by one slitmask pointing are listed in one row. All objects, including standard stars, were observed with the same set-up of the multislit unit. Resulting spectra of the GCs and of diffuse light are shown in Fig. 2. The detailed description of all reduction steps is given in Sharina et al. (2006). Here we briefly review major points of our reduction strategy. The basic data reduction was carried out using software packages within the Interactive Data Language (IDL). The subsequent data analysis was carried out in MIDAS. The data reduction included removing cosmics, bias subtraction, flat-field correction and correction of geometric field distortion. After wavelength calibration and sky subtraction, aperture windows in the direction of the spatial axis were defined, and the spectra were extracted by summing the two-dimensional spectra in the spatial direction. Then the spectra were corrected for atmospheric extinction and were flux calibrated. We use spectroscopic Lick standard stars, observed in the same night through the central slit of the slit mask, for flux calibration

Table 3. Journal of spectroscopic observations.

Object	Date	Exposure (s)	Seeing
NGC 147			
Hodge I, II, III	23/09/2003	3 × 900	1.2
NGC 185			
FJIII, IV, V, VI, VII	22/09/2003	4 × 900	1.2
FJJI, FJJII	26/09/2003	3 × 900	1.2
FJJVIII	26/09/2003	3 × 600	1.2
NGC 205			
Hubble II, V, VI, VII	23/09/2003	4 × 900	1.2
Hubble I	25/09/2003	900	1.2
Stars			
HD10307	25/09/2003	2 × 30	1.2
HD26784	26/09/2003	2 × 20	1.2
HD26757	26/09/2003	2 × 20	1.2
BD+26377	26/09/2003	2 × 30	1.2

of all spectra. In those nights when radial velocity standard stars were not observed, we use spectra of the twilight sky to compute radial velocities relative to telluric lines. In addition to the spectra of GCs, we analysed spectra of the diffuse galaxy light in the same way. These spectra were obtained near the cluster FJIII in NGC 185 and in fields f1–f5 in NGC 205 (see Fig. 2 for details).

2.2 Calibration of Lick indices

Before measuring indices, we degraded our spectra to the resolution of the Lick system, taking into account its wavelength-dependent resolution (Worthey & Ottaviani 1997). The effective resolution of our spectra has been determined using spectra of standard stars as a width (FWHM) of the corresponding autocorrelation function divided by $\sqrt{2}$ (Tonry & Davis 1979). The resolution-correction technique is described in detail in Puzia et al. (2002). Lick indices were measured on spectra corrected for radial velocities (Table 7), with a typical radial velocity error of $\sim$30 km s^{-1}. Chilingarian et al. (2005) measured radial velocities for GCs FJJIV and Hodge II according to our request using his method and obtained $V_h = -182 \pm 12$ and $V_h = -128 \pm 9$ km s^{-1}, correspondingly, in very good agreement with our measurements. The spectra of diffuse galactic light were corrected for velocity dispersion determined using algorithms of Tonry & Davis (1979). Broadening of lines in the spectra of diffuse galactic light due to velocity dispersion for the fields f1–f5 in NGC 205 and the field in NGC 185, accordingly, was obtained to be 1.5 ± 0.3, 1.5 ± 0.3, 1.4 ± 0.3, 1.3 ± 0.3, 1.3 ± 0.3, 1.1 ± 0.3 and 0.9 ± 0.5 Å. The velocity dispersion determined by us for the central parts of the galaxies is slightly larger than that from the literature (Carter & Sadler 1990; Bender, Paquet & Nieto 1991; Simien & Prugniel 2002), but still well within the errors. Table 4 summarizes zero-points of the linear transformation of our index measurements to the Lick/IDS standard system with the corresponding rms errors. We obtained these zero-points from observations of standard stars listed in Table 3. These zero-points coincide well within the errors with those obtained in other nights from observations of a large set of Lick standard stars with the multislit unit of the SCORPIO spectrograph equipped with a grism VPHG1200g which provides a spectral resolution $\sim$5 Å (Sharina, Afanasiev & Puzia 2006). Lick indices were measured using the code GONZO (Puzia et al. 2002).

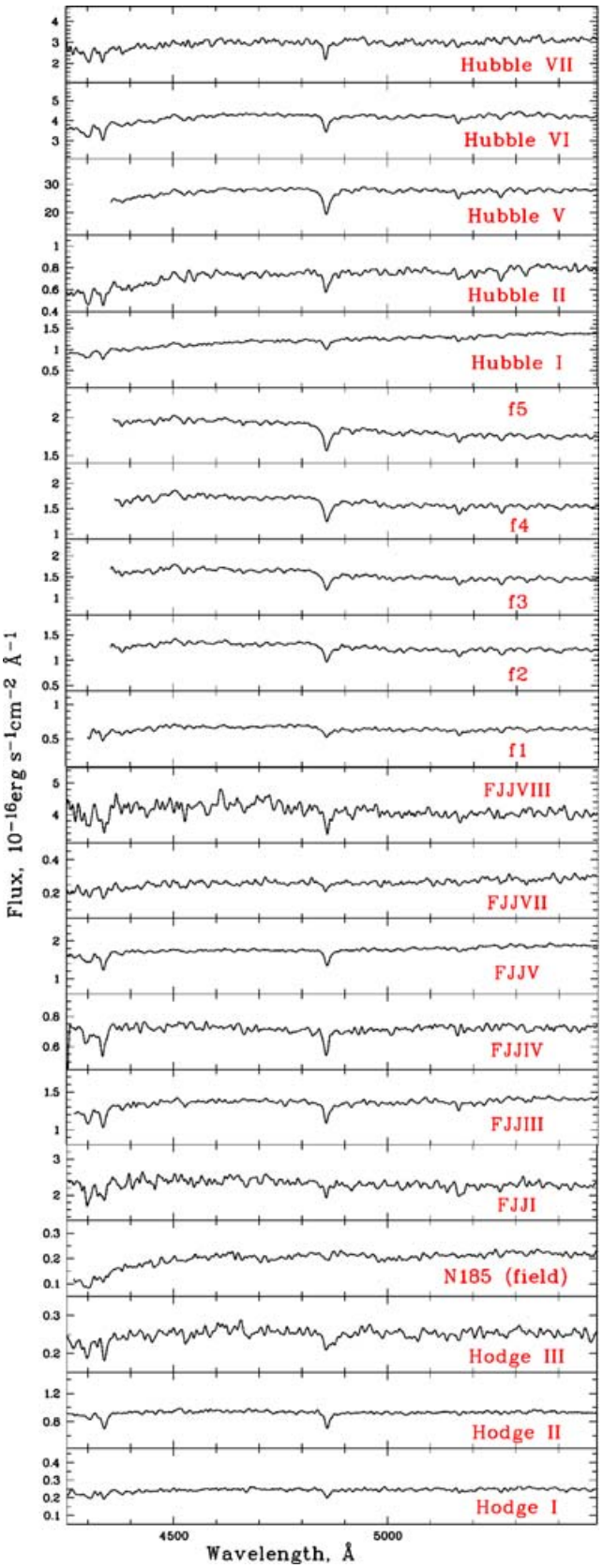

Figure 2. Flux calibrated spectra of GCs and diffuse light in NGC 147, 185 and 205 at a constant resolution of 8 Å at all wavelengths.

Table 4. Correction terms of the transformation to the Lick/IDS standard system Worthey et al. (1994). We applied them in the following way $I_{\rm Lick} = I_{\rm measured} + c$. The range of index values covered by our standard stars is shown in the fourth column.

Index	c	rms error	Index range	units
Ca4227	0.117	0.055	[0.03–0.8]	Å
G4300	0.520	0.332	[2.6–5.3]	Å
Fe4384	0.767	0.235	[2.3–4.0]	Å
Ca4455	0.851	0.136	[0.9–1.3]	Å
Fe4531	0.197	0.611	[2.2–2.7]	Å
Fe4668	−0.068	0.673	[2.2–3.8]	Å
Hβ	−0.024	0.197	[2.3–3.8]	Å
Fe5015	0.577	0.284	[3.4–4.2]	Å
Mg_1	0.009	0.008	[0.01–0.03]	mag
Mg_2	0.019	0.006	[0.08–0.16]	mag
Mgb	0.243	0.162	[1.9–3.0]	Å
Fe5270	0.223	0.546	[1.5–2.3]	Å
Fe5335	0.201	0.398	[1.4–1.7]	Å
Fe5406	0.120	0.049	[0.7–1.2]	Å
Hγ_A	−0.417	0.383	[0.4–2.4]	Å
Hγ_F	−0.191	0.364	[0.0–2.0]	Å

The Lick index uncertainties were determined from bootstrapping the object spectrum. All index values and the errors for observed GCs, diffuse-light fields, and combined spectra of GCs are presented in Tables 5 and 6.

2.3 Ages, metallicities and [α/Fe] ratios

In the following we compute ages, metallicities, [Z/H][1] and [α/Fe] for our sample GCs using the information acquired from the measurements of the Lick indices.

2.3.1 A three-dimensional interpolation and χ^2 minimization routine

We developed a program for age, metallicity and [α/Fe] determination which involves fitting all available Lick indices using the SSP model predictions of Thomas, Maraston & Bender (2004). Our three-dimensional linear interpolation routine obtains a full set of theoretical Lick indices from required ages, [Z/H] and [α/Fe] ratios by minimization of the χ^2 function:

$$\chi^2 = \sum_{i=1}^{N} \left[\frac{I_i - I_i(\text{age}, [\text{Z/H}], [\alpha/\text{Fe}])}{\sigma_{I_i}} \right]^2,$$

where N is the number of Lick indices involved in the analysis, I_i is an observed index, σ_{I_i} is the total uncertainty of the index, including rms error of transformations to the Lick/IDS system, $I_i(\text{age}, [\text{Z/H}], [\alpha/\text{Fe}])$ is the theoretical index prediction. The program computes 95 per cent confidence intervals and 1σ errors of ages, [Z/H] and [α/Fe]. Our routine works entirely within the three-dimensional space defined by the model grids. The ranges of estimated values are Age: [1, 15] Gyr, [Z/H] : [−2.25, 0.35] dex, and [α/Fe]: [0, 0.5] dex. The program makes determinations based on 100 combinations of initial conditions randomly distributed within this three-dimensional space, and the most frequent event is taken as a value of the global minimum. The errors in age, [Z/H] and [α/Fe] depend primarily on random index uncertainties and uncertainties of transformations to the Lick/IDS standard system.

To test our routine we compare ages, [Z/H] and [α/Fe] obtained by our program using the SSP model predictions from Thomas et al. (2004) with the ones available in the literature for 12 Galactic and 46 M31 GCs (see Fig. 3). We use the Lick index data for M31 GCs with measurement uncertainties $\Delta\text{H}\beta \leqslant 0.5$, $\Delta\text{H}\gamma_A \leqslant 0.7$, $\Delta\text{H}\delta_A \leqslant 0.7$, and $\Delta[\text{MgFe}]' \leqslant 0.4$ Å (see Puzia et al. 2005b) from Worthey (1994), Kuntschner et al. (2002), Beasley et al. (2004), and Puzia, Perrett & Bridges (2005a). The data on ages, [Z/H] and [α/Fe] for M31 GCs were taken from Puzia et al. (2005a), and the Lick index data for Galactic GCs from Puzia et al. (2002). When applying our fitting routine to these Lick index data we use all available indices except for CN1 and CN2. We found that CN1 and CN2 increase the 1σ errors of our results and can even skew them (see Proctor, Forbes & Beasley 2004). Fig. 3 demonstrates linear correlations between our determinations of age, metallicity and [α/Fe] and the corresponding data from the literature. We found the following linear relations: Age $_{\rm lit}$ = Age $_{\rm our}$ + 1.3 Gyr, $[\alpha/\text{Fe}]_{\rm lit} = [\alpha/\text{Fe}]_{\rm our}$ −0.02 dex, [Fe/H] $_{\rm lit}$ = 0.93 [Z/H] $_{\rm our}$ −0.2 dex for the sample of MW GCs, and [Z/H] $_{\rm lit}$ = 1.02 [Z/H] $_{\rm our}$ + 0.08 dex for M31 GCs.

Only three of the sample Galactic GCs have [α/Fe] measurements from high-resolution spectroscopy of stars in 45 Milky Way GCs by Pritzl, Venn & Irwin (2005). We find that our results for Galactic GCs are close to the literature data. However, the data for M31 GCs scatter relative to the best least-squares fit shown by a solid line on the third panel in Fig. 3 with a rms error ∼0.2 dex. More high-resolution spectroscopy of individual stars in young and of low-[α/Fe] GCs are needed to determine the real accuracy of our [α/Fe] determination method. It should be pointed out that the relative error Δ Age/Age is fairly constant at around 0.3. Unfortunately, there are no GCs with young ages and low-[α/Fe] in our comparison sample to check for potential biases in our spectroscopic age estimates. The middle panel of Fig. 3 shows a tight correlation between [Fe/H] data from Harris (1996) for Galactic GCs and our estimates. The existence of the tight correlation between [Fe/H] data for Galactic GCs and [Z/H] values from SSP models was also noticed by Thomas, Maraston & Korn (2003) and Proctor et al. (2004). Proctor et al. (2004) referred this result to problems in the calibration of the Lick indices or the metallicity scale in SSP models. According to our exercise the [Fe/H]–[Z/H] correlation is not a one-to-one relation.

2.3.2 Results

Resulting ages, metallicities and [α/Fe] ratios obtained with our routine for GCs, diffuse-light fields and the stacked spectra of GCs in NGC 147, 185 and 205 are listed in Table 7. 1σ uncertainties of our results for each object are summarized in Table 7.

For all studied GCs we construct age–metallicity and [α/Fe] diagnostic plots (see Fig. 4) similar to the techniques described in Puzia et al. (2005b). It is of interest to see whether the information coming from the age–metallicity plots coincides well with the results obtained by applying of our fitting routine. We use the SSP model predictions of Thomas et al. (2004) and an [α/Fe]-insensitive metallicity index $[\text{MgFe}]' = \{\text{Mg}b(0.72\,\text{Fe5270} + 0.28\,\text{Fe5335})\}^{1/2}$.

Inspection of Fig. 4 shows that for those GCs with multiple Balmer line indices the ages, metallicities and [α/Fe] ratios

[1] We use the standard definition, $[X/Y] = \log(X/Y) - \log(\text{X}_\odot/\text{Y}_\odot)$, where X and Y are masses of specific elements. A designation [Z/H] implies the overall metallicity.

Table 5. GC indices ($\lambda < 4700$ Å) (first line) corrected for zero-points of transformation to the standard system (Table 4) and errors determined from bootstrapping the object spectrum (second line). Approximate S/N per pixel measured at 5000 Å of the initial one-dimensional spectra, not degraded to the resolution of the Lick system are listed in the second column.

ID	S/N	Ca4227 (Å)	G4300 (Å)	Hγ_A (Å)	Hγ_F (Å)	Fe4383 (Å)	Ca4455 (Å)	Fe4531 (Å)	Fe4668 (Å)
Hodge I	20	0.15	3.41	0.10	1.27	2.53	0.42	0.91	0.16
		±0.05	±0.13	±0.42	±0.42	±0.19	±0.20	±0.24	±0.31
Hodge II	34	0.36	0.58	2.64	2.04	0.55	0.79	0.86	−0.44
		±0.02	±0.06	±0.25	±0.25	±0.10	±0.11	±0.13	±0.18
Hodge III	14	0.14	2.30	0.72	1.60	0.12	0.53	1.62	1.94
		±0.08	±0.21	±0.70	±0.71	±0.29	±0.32	±0.37	±0.51
All N147 GCs	43	0.30	1.39	1.35	1.80	1.05	0.66	1.08	−0.01
		±0.02	±0.04	±0.15	±0.15	±0.06	±0.07	±0.08	±0.11
FJJI	18	0.84	3.00	2.78	2.27	2.11	0.77	0.82	−1.41
		±0.09	±0.20	±0.62	±0.63	±0.32	±0.34	±0.37	±0.45
FJJIII	55	–	0.92	0.88	1.65	0.51	0.74	1.11	−0.21
		–	±0.05	±0.15	±0.16	±0.07	±0.08	±0.08	±0.12
FJJIV	30	–	1.02	2.32	2.17	0.69	0.84	−0.28	0.36
		–	±0.07	±0.29	±0.29	±0.12	±0.13	±0.16	±0.21
FJJV	70	–	1.75	2.05	2.06	0.93	1.15	1.21	−0.04
		–	±0.03	±0.12	±0.13	±0.05	±0.06	±0.07	±0.10
FJJVII	16	0.74	2.55	0.33	1.60	3.37	1.59	3.15	0.45
		±0.10	±0.20	±0.72	±0.73	±0.31	±0.33	±0.39	±0.58
FJJVIII	20	-0.12	1.61	2.08	1.91	1.12	0.46	1.06	0.70
		±0.07	±0.20	±0.63	±0.64	±0.34	±0.36	±0.40	±0.51
NGC185 field	27	–	–	–	1.21	0.88	1.76	0.97	0.02
		–	–	–	±0.06	±0.21	±0.24	±0.28	±0.36
FJJI + III + IV	106	–	–	1.70	2.05	1.22	0.68	1.21	−0.54
		–	–	±0.06	±0.06	±0.02	±0.03	±0.03	±0.04
All N147 GC + FJJI + III + IV + V + VIII	120	–	–	1.61	2.00	1.17	0.67	1.11	−0.47
				±0.05	±0.05	±0.02	±0.02	±0.03	±0.03
Hubble I	20	0.70	2.59	0.10	1.31	1.44	0.72	1.19	1.24
		±0.08	±0.18	±0.64	±0.65	±0.29	±0.30	±0.33	±0.46
Hubble II	86	0.33	2.47	0.53	1.53	1.82	1.14	1.82	0.08
		±0.00	±0.02	±0.07	±0.07	±0.03	±0.04	±0.04	±0.05
Hubble V	180	–	–	–	–	0.79	1.15	1.66	1.18
		–	–	–	–	±0.00	±0.01	±0.01	±0.01
Hubble VI	26	0.62	2.25	2.22	2.61	3.05	1.23	2.34	0.64
		±0.05	±0.11	±0.35	±0.35	±0.18	±0.19	±0.21	±0.26
Hubble VII	36	0.47	2.68	−0.03	1.42	1.52	0.55	1.76	−1.21
		±0.03	±0.07	±0.23	±0.23	±0.11	±0.12	±0.14	±0.17
Hubble I + VII	100	0.56	2.73	0.16	1.35	1.48	0.56	1.92	1.04
		±0.02	±0.05	±0.13	±0.14	±0.08	±0.08	±0.09	±0.11
Hubble VI + FJJVII	30	0.55	2.42	1.06	1.51	3.56	1.44	2.49	0.31
		±0.03	±0.07	±0.27	±0.27	±0.12	±0.13	±0.15	±0.20
NGC205 f1	130	–	–	–	–	2.08	1.44	1.78	2.87
		–	–	–	–	±0.04	±0.04	±0.05	±0.07
NGC205 f2	80	–	–	–	–	1.57	1.46	2.25	1.60
		–	–	–	–	±0.03	±0.04	±0.04	±0.06
NGC205 f3	76	–	–	–	–	1.83	1.26	2.54	3.06
		–	–	–	–	±0.04	±0.04	±0.04	±0.06
NGC205 f4	80	–	–	–	–	0.94	1.46	1.73	2.90
		–	–	–	–	±0.04	±0.04	±0.05	±0.06
NGC205 f5	54	–	–	–	–	3.02	1.46	1.39	2.27
		–	–	–	–	±0.05	±0.06	±0.07	±0.11
NGC205 f1, f2, f3	180	–	–	–	–	1.63	1.35	2.12	2.17
		–	–	–	–	±0.01	±0.01	±0.01	±0.02
NGC205 f4, f5	100	–	–	–	–	2.41	1.57	1.54	2.64
		–	–	–	–	±0.03	±0.03	±0.03	±0.04

derived from different diagnostic plots are consistent with each other. The location of objects in these diagrams correspond well with our fitting results (Table 7). The problem of age determination for very metal-poor GCs arises, first, since the model lines cross in this region, and, secondly, because GCs tend to fall below the oldest model sequence (see Covino, Galletti & Pasinetti 1995).

Our results reveal solar [α/Fe] ratios for most of our sample GCs, which is consistent with slow and/or extended GC/star formation

Table 6. GC indices ($\lambda > 4700$ Å) (first line) corrected for zero-points of transformation to the standard system (Table 4) and errors determined from bootstrapping the object spectrum (second line).

GC name	Hβ (Å)	Fe5015 (Å)	Mg1 (mag)	Mg2 (mag)	Mgb (Å)	Fe5270 (Å)	Fe5335 (Å)	Fe5406 (Å)
Hodge I	2.71	1.48	0.013	0.076	0.67	1.07	0.35	−0.55
	±0.31	±0.34	±0.009	±0.009	±0.37	±0.37	±0.38	±0.38
Hodge II	3.13	1.14	0.012	0.029	0.62	0.65	0.74	0.17
	±0.18	±0.21	±0.005	±0.005	±0.23	±0.23	±0.24	±0.24
Hodge III	1.92	0.09	0.008	0.031	0.32	0.94	0.69	0.36
	±0.52	±0.58	±0.015	±0.015	±0.64	±0.66	±0.67	±0.68
All N147 GCs	2.85	1.24	0.015	0.046	0.66	0.97	0.61	−0.02
	±0.11	±0.12	±0.003	±0.003	±0.14	±0.14	±0.14	±0.14
FJJI	2.00	1.04	0.003	0.077	2.09	0.97	−0.13	0.86
	±0.46	±0.51	±0.015	±0.015	±0.55	±0.56	±0.57	±0.57
FJJIII	2.40	2.59	0.003	0.057	0.79	0.60	0.75	0.45
	±0.12	±0.13	±0.003	±0.003	±0.14	±0.14	±0.15	±0.15
FJJIV	2.70	0.61	−0.026	0.018	0.78	0.35	0.75	-0.00
	±0.21	±0.24	±0.005	±0.005	±0.26	±0.26	±0.27	±0.27
FJJV	2.73	1.94	0.010	0.048	0.60	0.63	0.41	0.37
	±0.10	±0.11	±0.002	±0.002	±0.12	±0.12	±0.12	±0.12
FJJVII	2.91	2.65	0.020	0.056	1.31	1.85	2.16	0.37
	±0.59	±0.63	±0.016	±0.016	±0.66	±0.67	±0.68	±0.69
FJJVIII	2.47	2.22	0.022	0.057	1.11	1.15	−0.37	0.32
	±0.51	±0.54	±0.014	±0.014	±0.59	±0.60	±0.60	±0.60
NGC185 field	2.08	3.65	0.053	0.066	0.73	−0.68	1.40	0.77
	±0.37	±0.42	±0.010	±0.010	±0.45	±0.46	±0.47	±0.48
FJJI + III + IV	2.37	1.77	0.011	0.058	0.99	0.90	0.02	0.18
+ V + VIII	±0.04	±0.05	±0.001	±0.001	±0.05	±0.05	±0.05	±0.06
All N147 GC	2.41	1.65	0.012	0.057	0.94	0.85	0.13	0.14
+ FJJI + III + IV	±0.04	±0.04	±0.001	±0.001	±0.04	±0.04	±0.04	±0.04
+ V + VIII								
Hubble I	2.66	3.31	0.030	0.067	1.29	1.08	1.08	0.61
	±0.47	±0.52	±0.013	±0.014	±0.57	±0.58	±0.59	±0.60
Hubble II	2.32	2.75	0.017	0.071	1.23	1.17	1.09	0.68
	±0.05	±0.06	±0.002	±0.002	±0.06	±0.06	±0.06	±0.06
Hubble V	4.14	3.06	0.013	0.069	1.35	1.69	1.31	0.88
	±0.01	±0.01	±0.000	±0.000	±0.02	±0.02	±0.02	±0.02
Hubble VI	3.12	2.21	0.014	0.080	1.42	2.51	1.88	0.62
	±0.27	±0.29	±0.008	±0.008	±0.31	±0.31	±0.32	±0.32
Hubble VII	2.39	2.16	0.011	0.070	1.18	0.94	0.45	0.58
	±0.18	±0.19	±0.005	±0.005	±0.21	±0.21	±0.21	±0.22
Hubble I + VII	2.60	2.90	0.043	0.081	0.62	0.53	0.62	0.45
	±0.11	±0.12	±0.003	±0.003	±0.12	±0.12	±0.13	±0.13
Hubble VI + FJJVII	2.86	2.82	0.016	0.073	1.56	2.09	1.82	0.72
	±0.21	±0.22	±0.006	±0.006	±0.24	±0.24	±0.25	±0.25
NGC205 f1	3.36	3.58	0.042	0.091	1.74	0.78	1.18	1.08
	±0.07	±0.08	±0.002	±0.002	±0.09	±0.09	±0.09	±0.10
NGC205 f2	3.86	4.03	0.031	0.081	1.81	1.67	1.34	1.04
	±0.06	±0.07	±0.002	±0.002	±0.08	±0.08	±0.09	±0.09
NGC205 f3	3.60	3.25	0.018	0.079	1.76	1.78	1.86	1.42
	±0.06	±0.07	±0.002	±0.002	±0.08	±0.08	±0.09	±0.09
NGC205 f4	3.30	3.51	0.037	0.081	1.53	1.69	1.20	1.15
	±0.06	±0.07	±0.002	±0.002	±0.09	±0.09	±0.09	±0.09
NGC205 f5	2.81	2.53	0.012	0.094	1.49	1.05	2.02	0.77
	±0.11	±0.12	±0.003	±0.003	±0.13	±0.14	±0.14	±0.14
NGC205 f1, f2, f3	3.45	3.42	0.024	0.078	1.66	1.62	1.37	1.07
	±0.02	±0.02	±0.000	±0.001	±0.03	±0.03	±0.03	±0.03
NGC205 f4, f5	3.12	3.21	0.029	0.091	1.43	1.37	1.47	0.93
	±0.04	±0.05	±0.001	±0.001	±0.06	±0.06	±0.06	±0.06

histories in their host dSph galaxies. Low [α/Fe] enhancements were also found in individual red giant stars in dwarf spheroidal galaxies (dSph) with high-dispersion spectroscopy (e.g. Shetrone, Bolte & Stetson 1998; Smecker-Hane & McWilliam 1999; Bonifacio et al. 2000; Shetrone et al. 2001; Shetrone et al. 2003; Tolstoy et al. 2003; Geisler et al. 2005). Shetrone et al. (2001) and Tolstoy et al. (2003) suggested that the low abundance ratios at low metallicities could result from a slow star formation rate. Tolstoy

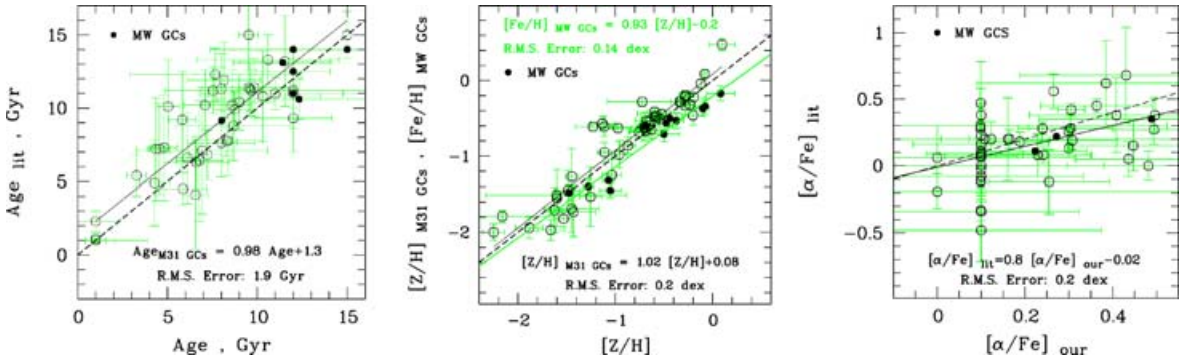

Figure 3. Age, [Z/H] and [α/Fe] ratios obtained with our fitting routine (see Section 2.3) for Galactic GCs (filled circles) using the Lick index data of Puzia et al. (2002) are compared with the ages obtained from CMD studies (Salaris & Weiss 2002), [Fe/H] data from Harris (1996) and [α/Fe] values from Pritzl et al. (2005). Age, [Z/H] and [α/Fe] obtained in this work with our code for M31 GCS (open circles) using the Lick index data from Worthey et al. (1994), Kuntschner et al. (2002), Beasley et al. (2004) and Puzia et al. (2005a) are compared with ages, [Z/H] and [α/Fe] from Puzia et al. (2005a). Dashed lines show the one-to-one relation. Solid lines indicate the least-squares fit to the data.

et al. suggested that dSph galaxies experienced a fairly uniform chemical evolution despite their different star formation histories. This conclusion was backed by theoretical model predictions (see e.g. Lanfranchi & Matteucci 2003).

Suppose that our three samples of GCs with measured ages, [Z/H] and [α/Fe] ratios in NGC 147, 185 and 205 were drawn from the same normally distributed parent populations. To check the hypothesis we compare our three samples in pairs and apply the F-test (comparison of variances) and Student's t-test (comparison of means) (see e.g. Stuart & Ord 1994). The results of our statistical tests are summarized in Table 8. The F-test shows that at a significance level of 5 per cent the variances are equal. That is the quotient of two variances is always less than the corresponding critical value of F-distribution. We compute the T-statistics $T = t_{1-p}s\sqrt{1/n_1 + 1/n_2}$, where t_{1-p} is a critical value of T-distribution at a significance level of $1 - p$; n_1 and n_2 are numbers of degrees of freedom in the first and the second samples, and s is a mean weighted variance $s^2 = [(n_1 - 1)\, s_1^2 + (n_2 - 1)\, s_2^2]/(n_1 + n_2 - 2)$, where s_1 and s_2 are variances for the two samples. One can see from Table 8 that the difference between mean values for the three samples taken in pairs is always less than the corresponding T value. Hence, at a significance level of 5 per cent the [α/Fe] enhancements for the studied GCs in NGC 147, 185 and 205 have similar approximately zero values.

2.3.3 Individual globular cluster systems

NGC 205. We stack the spectra of the diffuse galaxy in NGC 205 in order to achieve a higher signal-to-noise ratio (S/N). The measurements for fields f1–f5 are indicated by open circles in Fig. 4. Large open circles in the top and middle left-hand panels of Fig. 4 illustrate the Lick index values for averaged spectra for the fields of diffuse light in NGC 205: f1 + f2 + f3 and f4 + f5. Measurements for the combined spectrum for the clusters Hubble I + Hubble VII are shown as large filled circle.

It is clear from the Hβ diagnostic plot in the upper left-hand panel of Fig. 4 and from Table 7 that the central GC in NGC 205, Hubble V and its surrounding fields f1, f2, f3 are consistent with the youngest ages in NGC 205 and in our entire sample. However, the metallicity of Hubble V appears to be lower than that of the surrounding fields. On the other hand, the second nearest GC to the optical centre of NGC 205, Hubble VI, has about the same metallicity but an older age relative to the very central stellar population. Finally, the more metal-poor GCs Hubble I, Hubble II, and Hubble VII are the oldest GCs in NGC 205. All three clusters are located at large galactocentric distances. Hence, our measurements show that there is a tendency of increasing age with increasing galactocentric distance for stellar populations in NGC 205. This fact is confirmed by extensive CMD studies of stellar populations in NGC 205 as it will be shown in Section 4.3.

NGC 185. This galaxy hosts eight off-centre GCs. All of them are located at the projected distance $d_{\rm proj}$ = [0.6–1.0] kpc from the optical centre of the galaxy, except FJJIII with $d_{\rm proj}$ = 0.2 kpc. Fig. 4 shows that all observed GCs in NGC 185 are old and metal-poor with the exception of FJJVII, which appears to be the youngest and most metal-rich GC in NGC 185 (see Table 7). FJJVII has approximately the same age and metallicity as Hubble VI in NGC 205 according to our measurements. The diagnostic plots and Table 7 show that the stacked spectrum of these two clusters shows the same intermediate-age and metallicity. Those two GCs may have formed some 4–6 Gyr ago. It will be shown in Section 4.2 that similar intermediate-age and metallicity GCs exist in the halo of M31.

NGC 147. All three observed GCs in NGC 147 are old and metal-poor, similar to what is found for GCs in NGC 185. It can be seen in Fig. 4 that the chemical compositions obtained from the stacked spectra for all GCs except FJJVII in NGC 185 (filled square), NGC 147 (filled diamond) and GCs Hubble I, and VII in NGC 205 (filled circle), as well as for all old and low metallicity GCs in NGC 185 and 147 (filled triangle), coincide within the errors.

3 STELLAR PHOTOMETRY DATA

3.1 Data reduction

In order to test whether our spectroscopic results are consistent with fundamental parameters derived from CMDs, we search the *HST* archive for available photometry for our sample GCs. Table 9 summarizes the result of our search, which recovered useful WFPC2 data for eight GCs. We use the HSTPHOT package (Dolphin 2000a) to perform stellar photometry and artificial star tests. We use the charge transfer efficiency and zero-point magnitude correction derived by Dolphin (2000b). Stars with S/N > 5, $|\chi| < 20$, and $|sharpness| > 0.4$, were eliminated from the final photometry list. The

Table 7. Ages, [α/Fe] and [Z/H] for GCs and diffuse-light regions for our sample galaxies. The values were obtained using our fitting routine of three-dimensional interpolation and χ^2 minimization (see Section 2.3 for details). Radial velocities measured by us with a typical error of about 30 km s^{-1} and approximate projected galactocentric distances based on the distance estimates from Table 1 are listed in the last two columns.

Object	Age (Gyr)	[α/Fe] (dex)	[Z/H] (dex)	V_h (km s^{-1})	$D_{\rm proj}$ (kpc)
NGC 147					
Hodge I	9 ± 3	0.1 ± 0.3	-1.2 ± 0.2	-107	0.0
Hodge II	8 ± 2	0.1 ± 0.3	-1.8 ± 0.2	-118	0.6
Hodge III	10 ± 3	0.5 ± 0.4	-1.5 ± 0.2	-201	0.3
All N147 GCs	9 ± 1	0.0 ± 0.3	-1.6 ± 0.1		
NGC 185					
FJJI	9 ± 4	0.3 ± 0.3	-1.2 ± 0.2	-264	0.7
FJJIII	10 ± 2	0.1 ± 0.3	-1.6 ± 0.3	-290	0.3
FJJIV	9 ± 2	0.0 ± 0.2	-2.0 ± 0.3	-157	0.8
FJJV	9 ± 2	0.0 ± 0.3	-1.5 ± 0.2	-370	0.9
FJJVII	7 ± 3	0.0 ± 0.3	-0.8 ± 0.2	-217	1.0
FJJVIII	8 ± 4	0.0 ± 0.5	-1.5 ± 0.3	-148	1.0
FJJVII + Hubble VI	5 ± 2	0.0 ± 0.3	-0.8 ± 0.2		
FJJI + III + IV + V + VIII	9 ± 2	0.3 ± 0.2	-1.6 ± 0.2		
Field	8 ± 5	0.1 ± 0.4	-1.1 ± 0.2	-206	0.3
All N147 GC + FJJI + III + IV + V + VIII	10 ± 2	0.3 ± 0.2	-1.7 ± 0.1		
NGC 205					
Hubble I	7 ± 2	0.2 ± 0.2	-1.1 ± 0.1	-144	1.0
Hubble II	10 ± 2	0.0 ± 0.2	-1.2 ± 0.1	-235	0.7
Hubble V	1.2 ± 0.6	0.0 ± 0.1	-0.6 ± 0.2	-212	0.0
Hubble VI	4 ± 2	0.0 ± 0.2	-0.8 ± 0.2	-170	0.3
Hubble VII	11 ± 2	0.1 ± 0.2	-1.3 ± 0.1	-189	0.4
Hubble I + VII	10 ± 2	0.1 ± 0.2	-1.2 ± 0.1		
f1	1.9 ± 0.8	0.0 ± 0.2	-0.5 ± 0.3	-245	0.05
f2	1.2 ± 0.8	0.0 ± 0.2	-0.4 ± 0.3	-230	0.07
f3	1.6 ± 1.1	0.0 ± 0.2	-0.5 ± 0.3	-238	0.07
f4	1.8 ± 1	0.5 ± 0.4	-0.6 ± 0.3	-216	0.10
f5	6 ± 5	0.0 ± 0.2	-0.8 ± 0.2	-226	0.12
f1 + f2 + f3	1.6 ± 0.8	0.0 ± 0.2	-0.5 ± 0.2		
f4 + f5	4 ± 2	0.0 ± 0.2	-0.7 ± 0.2		

uncertainty of transformations from the WFPC2 instrumental system to the standard Johnson–Cousins system contains many factors. The most important of them are uncertainties of photometric zero-points ($\sim$0.003 mag for the F555W filter, $\sim$0.002 mag for F814W filter), the CTE correction ($\sim$0.01 mag) and the aperture corrections ($\sim$0.05 mag; Dolphin 2000b).

3.2 Colour–magnitude and Hess diagrams

In order to avoid crowding we analyse in the following only GCs imaged with the PC chip (0.0455 arcsec pixel^{-1}). One exception is the cluster Hodge II which is located in a very sparse field of NGC 147 and is imaged with the WF3 chip of WFPC2. However, the surrounding field of this cluster is sparse enough to provide reliable stellar photometry. In general, photometric data for GCs imaged with lower resolution and/or located in the central dense regions of the galaxies reveal too high photometric errors to confidently determine ages and [Fe/H]. We calculate absolute stellar magnitudes using reddening and distance estimates listed in Table 1.

Fig. 5 shows CMDs and Hess diagrams for stars within the $R_{\rm GC}$ radius for *all* our sample GCs.[2] We consider the radius of a GC to be defined by the full area occupied by the bluest stars (old HB stars). To illustrate how $R_{\rm GC}$ was derived, we demonstrate spatial distribution of blue stars in the GC FJJI along X-axis (Fig. 6). Blue stars with $V - I < 0.2$ were selected in a 200×800 pixel rectangular area centred on the cluster. The distribution shows a clear maximum towards the centre of the cluster. Similar distributions were constructed for each of the studied clusters in X and Y directions, and the determined two values of $R_{\rm GC}$ were averaged. We adopt the size roughly 10–20 per cent smaller than the full area outlined by blue stars to reduce contamination effects. This area roughly corresponds to $R_{\rm GC}$ at a level of the number of blue stars: $N_{\rm back} + \sigma(N)$, where $N_{\rm back}$ is the mean number of blue stars around the studied cluster, and $\sigma(N)$ is the s.d. of this number. Structural parameters of GCs in NGC 205, 185 and 147 will be studied in our follow-up paper. Here we note that the sizes of the clusters measured using the distributions of blue stars are $\sim$3–4 times larger than the corresponding effective radii. For example, FJJI has $r_{\rm e} = 1.2$ arcsec, whereas its $R_{\rm GC}$ is $\sim$4.6 arcsec. It should be noted that central regions of the clusters do not show the presence of resolved stars which pass our goodness-of-fit criteria. This fact was taken into account in selection of field stars surrounding a cluster. The area for selection of such stars was computed as $S' = \pi\,(R_{\rm GC}^2 - R_{\rm c}^2)$, where $R_{\rm GC}$ is the radius of a GC determined via spatial distribution of blue stars and $R_{\rm c}$ is the radius of the central unresolved area.

Fig. 5 consists of four panels for each GC. An uncleaned CMD for stars within $R_{\rm GC}$ of each GC is illustrated in the left-hand panel. Empirical loci of RGBs for Galactic GCs are shown for comparison (Lee et al. 1993). CMDs for field stars from an equal area is shown in the second panel. The third panel represents the difference between recovered magnitude and input magnitude for recovered stars obtained from artificial star tests. It is clear that systematic effects do not exceed 0.05 mag for stars with the completeness limit of $>$50 per cent, which is indicated by a dotted line. Given the quality of the data we are able to estimate the HB morphology index (see below) with a high level of confidence.

The fourth panel represents Hess diagrams after decontamination from the field contribution. The statistical field subtraction was done in the following way. (1) We constructed a Hess diagram for stars within $R_{\rm GC}$ of each GC. (2) Similar Hess diagrams were obtained for stars surrounding the corresponding GC. To take into account statistical fluctuations of the number of stars we consider stars in an annulus around the studied cluster. Our simulations show that four separate areas around the studied cluster are representative enough to construct Hess diagrams for field stars, which alleviates the problems of constructing background samples when a GC is located near to the image edge. (3) A mean Hess diagram was computed from these four Hess diagrams. (4) A cleaned Hess diagram was calculated as a difference between the contaminated Hess diagram and the mean Hess diagram for field stars. Positive data indicate the locus of GC stars in the cleaned Hess diagram. Solid lines represent the fundamental zero-age horizontal branches (ZAHBs) and isochrones taken from the Victoria-Regina stellar models of Vanden-Berg et al. (2006). Corresponding ages and metallicities are listed in Table 9.

[2] The figures for each GC can be downloaded from the anonymous ftp site: ftp.sao.ru (directory:/pub/sme/GCsM31dEs).

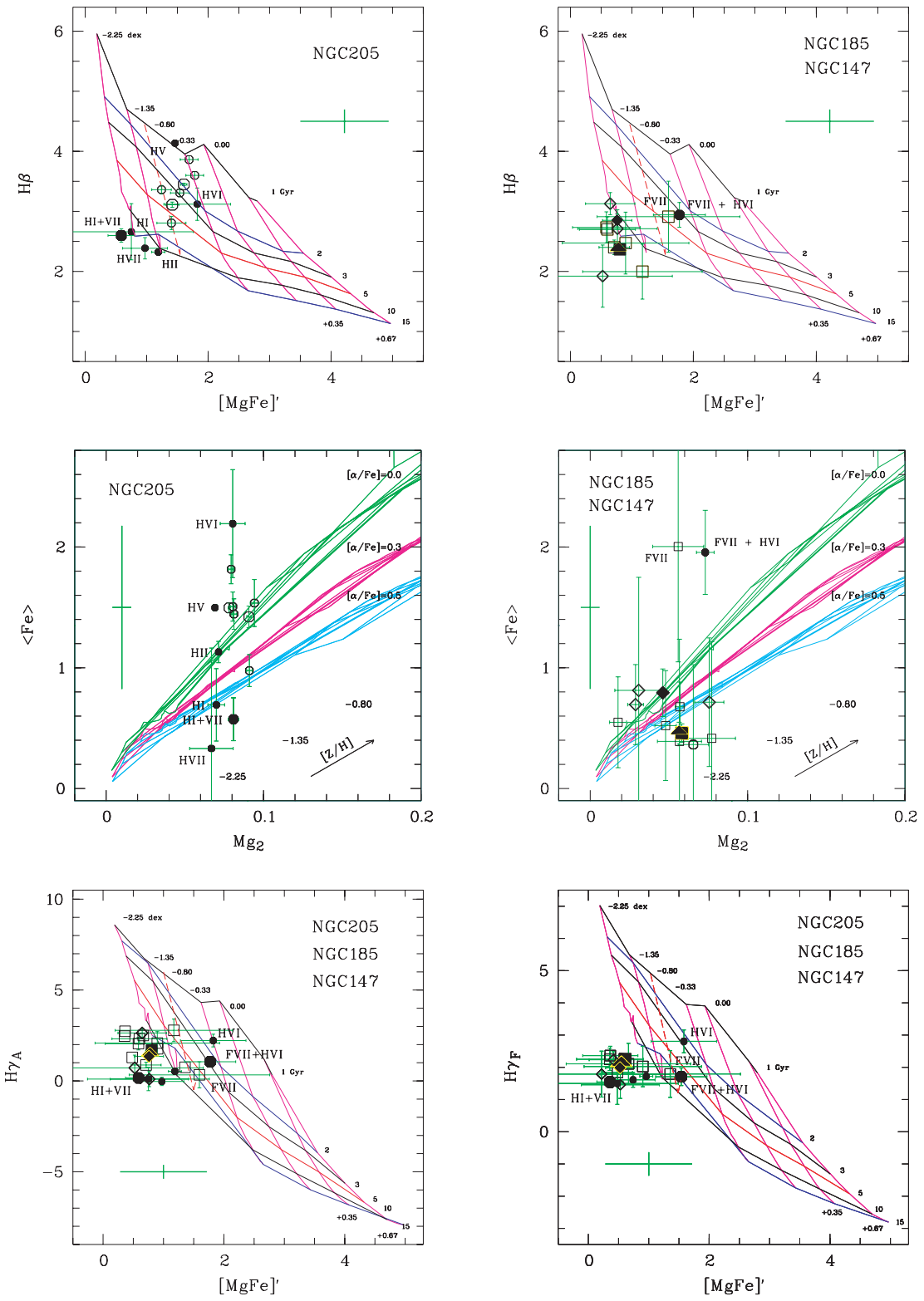

Figure 4. Diagnostic plots for GCs in NGC 205 (solid small circles), NGC 185 (open squares), NGC 147 (open diamonds), diffuse-light fields (open circles), and combined spectra of Hubble I + VII (large filled circle), FJJVII + Hubble VI (large filled circle), spectra of FJJI + III + IV + V + VIII (filled square), all GCs in NGC 147 (filled diamond), all GCs in NGC 147 and NGC 185, except FJJVII (filled triangle), and combined spectra diffuse-light fields f1 + f2 + f3 and f4 + f5 in NGC 205 (large open circles). The bootstrap errors from Table 5 are overplotted. We use the SSP model predictions from Thomas et al. (2003, 2004). Error bars on each plot show rms errors of the transformations to the Lick system (Table 4).

Table 8. Student's *t*-test and *F*-test statistics quantifying the probability that [α/Fe] ratios for GCs in NGC 147, 185, and 205 were drawn from the same distribution. Columns contain the following data: (2) numbers of degrees of freedom, (3) variances of [α/Fe] ratios, (4) critical values of *F*-distribution at a significance level of 5 per cent for the three samples taken in pairs, (5) mean [α/Fe] ratios, (6) *T*-statistics and (7) critical values of *T*-distribution at a significance level of 5 per cent for the three samples taken in pairs.

Galaxy	N	s^2	$F_{0.95}$	$\langle[\alpha/\mathrm{Fe}]\rangle$	T	$t_{0.95}$
NGC 205 (1)	5	0.008	$5.0^{1,2}$	0.06	$0.11^{1,2}$	1.80
NGC 185 (2)	6	0.012	$19.3^{2,3}$	0.07	$0.24^{2,3}$	1.86
NGC 147 (3)	2	0.05	$19.3^{1,3}$	0.23	$0.20^{1,3}$	1.90

3.3 Comparison with Victoria-Regina models

To fit theoretical isochrones to our stellar photometry data we use the ages, [Z/H] and [α/Fe] obtained in our spectroscopic study. We note that [α/Fe] = 0 was adopted for all studied GCs according to our spectroscopic results (see Section 2.3). Pipino, Matteucci & Chiappini (2006) adopted a relation [Fe/H] = [Z/H] −0.94 [α/Fe] for Thomas et al. (2003) SSP models on the basis of a calibration on Galactic GCs. Since we found that GCs in NGC 147, 185 and 205 have approximately solar [α/Fe], it means that [Fe/H] $\approx$ [Z/H] in our case. We have no spectroscopic data for Hubble VIII and FJJII. As a starting point for the spectroscopy–CMD comparison we adopt for these two clusters the age, metallicity and [α/Fe] values obtained from the averaged spectra of Hubble I + VII and all GCs in NGC 185.

To show how the choice of different isochrones affects our results we plot isochrones and ZAHBs (VandenBerg et al. 2006) for different [Fe/H] and [α/Fe] (Fig. 7), and adopt the age of 10 Gyr. The isochrones and ZAHBs for Age = 10 Gyr, [Fe/H] = −1.61 and [α/Fe] = 0 are drawn by grey lines. The difference in $(V-I)$ between isochrones that differ by 2 Gyr is of the order of a few hundredth of a magnitude. So, if we know the metallicity and [α/Fe], the typical error of age determinations for the GCs studied photometrically is ∼2 Gyr given the accuracy of our photometry and the scatter of the data for individual red giant stars relative to fitted isochrones. However, since the accuracy of our spectroscopic metallicity and [α/Fe] determinations is low in some cases, the uncertainties of the transformations into the standard VI system are ∼0.05 mag, and due to the effect of age–metallicity degeneracy on the colour of the RGB (e.g. Saviane et al. 2000; Dolphin et al. 2003), we estimate the error of our photometric age determinations to be $\lesssim$4 Gyr.

For all GCs, except Hubble II in NGC 205, the ages, metallicities and [α/Fe] ratios derived by measuring the Lick indices provide a good correspondence between the loci of RGB and HB stars and the theoretical models. The HB stars in Hubble II seem too bright for their metallicity, whereas the loci of RGB stars agree well with the spectroscopically derived metallicity. Our analysis indicates that in order to achieve good agreement between our spectroscopic and photometric results we have to reduce the distance modulus to NGC 205, $(m-M)_0 = 24.58$ (McConnachie 2004), by 0.2 mag. The resulting distance modulus is given in Table 1. The same distance modulus was applied to Hubble VIII in NGC 205.

There is a $\sim 2\sigma$ discrepancy between our spectroscopic ([Z/H] = -1.24 ± 0.17) and photometric (-1.6 ± 0.2) metallicity estimates for FJJI. We adopt a mean value for this cluster [[Z/H] = -1.4 ± 0.2 which coincides with a value obtained by Da Costa & Mould (1988).

3.4 Horizontal branch morphology

Blue HB (BHB) and red HB stars (RHB) in our sample GCs were selected according to the boxes marked in Fig. 5. The boundaries of the instability strip in the *V*, *I* filter set were taken from Harbeck et al. (2001): $(V-I)_0 = 0.4$–0.75. We determine the HB morphology index $(B-R)/(B+V+R)$ (Zinn et al. 1993) for each cluster. The resulting HB morphology indices are listed in Table 9. Errors of the HB morphology indices were determined by taking into account variations of a number of blue and red HB stars in the field regions. All GCs studied here appear to contain a significant population of BHB stars within their R_{GC} radius.

4 DISCUSSION

4.1 The second parameter effect

The morphology of the HB and the mean luminosity of the HB stars depend primarily on metallicity. Age is suspected to be the 'second parameter' (Lee, Demarque & Zinn 1994). In general, metal-poor old GCs have blue HBs and metal-rich 1–2 Gyr younger clusters

Table 9. Stellar photometry observations. The columns contain the following data: (1) name of the object (the index 's' marks targets for which spectra were obtained); (2) equatorial coordinates in J2000; (3), (4) and (5) source information from the *HST* archive; (6) and (7) [Fe/H] and age obtained by fitting theoretical isochrones and ZAHBs of VandenBerg et al. (2006) to our data; (8) the HB morphology index; (9) search radius inside which we consider stars as members of a particular GCs.

Object	RA (J2000) Dec. ($^{\mathrm{h}}$ $^{\mathrm{m}}$ $^{\mathrm{s}}$) ($^\circ$ $'$ $''$)	Filter, chip	Data set	Exposure time (s)	[Fe/H] (dex)	age (Gyr)	$\frac{B-R}{B+V+R}$	R_{GC} (arcsec)
NGC 147								
Hodge $\mathrm{II_s}$	00 33 15.20 +48 27 23.2	F555W, F814W, 3	U2OB01	4 × 1300, 4 × 1300	-2.0 ± 0.1	10	1:	4.8
NGC 185								
$\mathrm{FJJI_s}$	00 38 42.90 +48 18 41.2	F555W, F814W, PC	U3KL01	3 × 2800, 2 × 1300	-1.6 ± 0.2	10	0.2 ± 0.2	4.6
FJJII	00 38 48.30 +48 18 17.0	F555W, F814W, PC	U3KL02	3 × 2800, 2 × 1300	-2.1 ± 0.2	10	-0.2 ± 0.2	3.5
$\mathrm{FJJIII_s}$	00 39 03.90 +48 19 58.2	F555W, F814W, PC	U3KL03	3 × 2800, 2 × 1300	-2.0 ± 0.1	10	0.5 ± 0.3	4.1
$\mathrm{FJJIV_s}$	00 39 12.38 +48 22 49.2	F555W, F814W, PC	U3KL04	3 × 2800, 2 × 1300	-2.0 ± 0.2	10	0.7 ± 0.2	3.5
$\mathrm{FJJV_s}$	00 39 13.58 +48 23 05.8	F555W, F814W, PC	U3KL04	3 × 2800, 2 × 1300	-1.5 ± 0.1	10	0.9 ± 0.1	4.0
NGC 205								
Hubble $\mathrm{II_s}$	00 40 33.81 +41 39 40.2	F555W, F814W, PC	U3KL06	3 × 2800, 2 × 1300	-1.3 ± 0.1	10	-0.2 ± 0.3	3.2
Hubble VIII	00 39 53.99 +41 47 19.2	F555W, F814W, PC	U3KL10	3 × 2800, 2 × 1300	-1.8 ± 0.2	10	0.7 ± 0.2	3.8

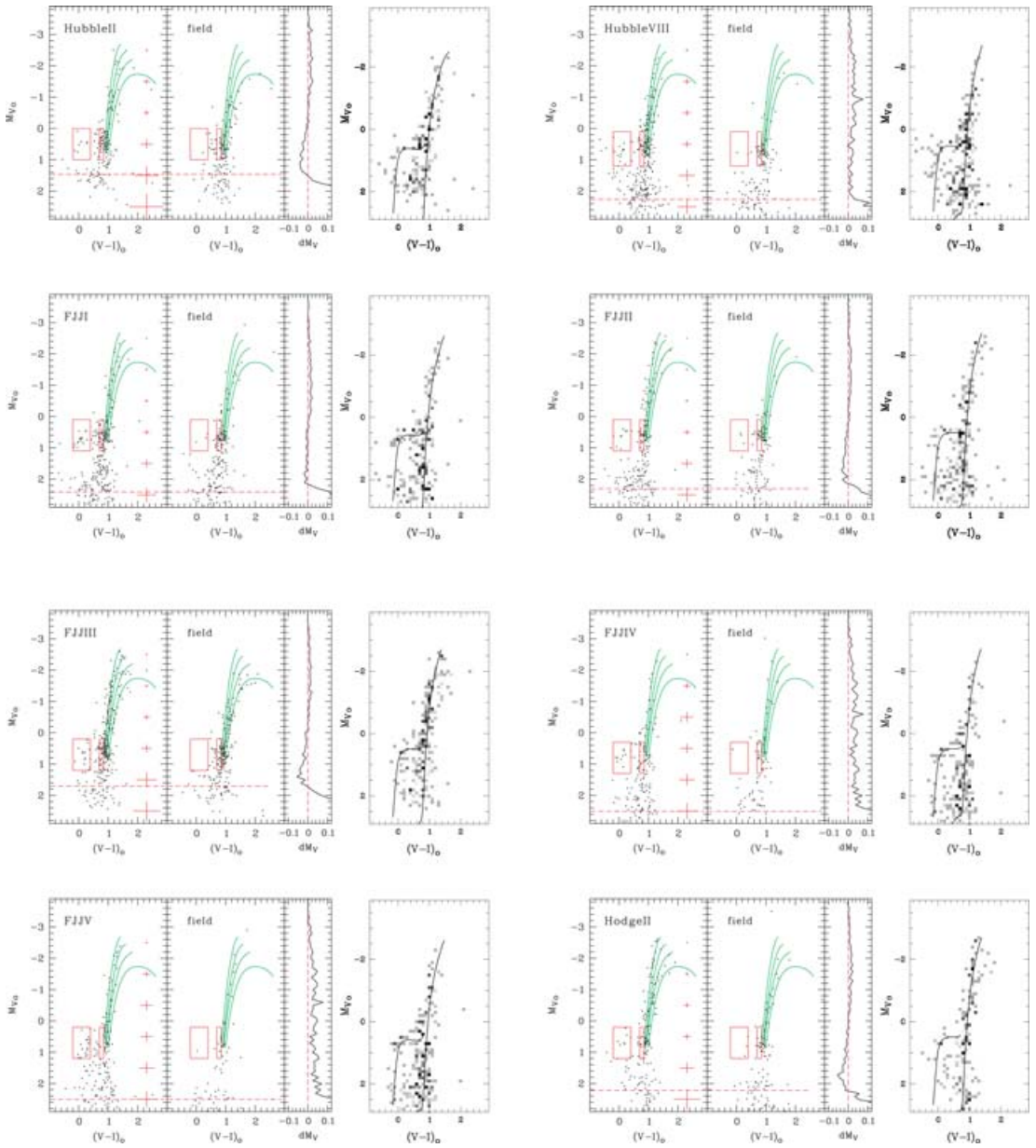

Figure 5. Stellar photometry results. From left- to right-hand side four panels for each cluster show the following data: (1) uncleaned CMD within the radius of each GC; (2) CMD for field galactic stars from the equal area; (3) difference between recovered magnitude and input magnitude for recovered star obtained from HSTPHOT artificial star tests; (4) Hess diagram after decontamination from the field contribution. Dashed line on the first and second panels indicates 50 per cent detection limit. Empirical loci of the RGB for Galactic GCs and photometric errors from artificial star tests are shown in the first panel. The GCs M15, M2, NGC1851 and 47 Tuc have metallicities [Fe/H] $= -2.17, -1.58, -1.29$ and -0.71 dex, respectively (Lee et al. 1993). The BHB and RHB stars in GCs are selected according the boxes. Isochrones and ZAHBs of VandenBerg et al. (2006) for ages, [Fe/H] and [α/Fe] indicated in Table 7 are shown in the fourth (right-hand) panel.

have predominantly red HBs. However, it is known that more parameters may influence the HB morphology such as helium abundance, CNO abundance, etc. (Lee et al. 1994). We suggest that the photometric data presented in our paper are accurate enough to consider the influence of age and metallicity on the HB morphology and to compare this effect with the one studied in the literature for GCs in our Milky Way and other nearby galaxies.

Fig. 8 shows the HB-type versus metallicity diagram for our eight sample GCs studied photometrically. The overplotted isochrones were taken from Rey et al. (2001). It can be seen that the HB morphologies for six of eight of our sample GCs follow the same behaviour as a function of metallicity as the 'young halo' Galactic GCs. Mackey & Gilmore (2004b) performed a comparison between 'old halo', 'young halo' and 'bulge/disc' Galactic GC subpopulations (Zinn 1993) using the HB-type versus metallicity diagram. The authors showed that the majority of external GCs are indistinguishable from Galactic young halo GCs. Our analysis shows that six of our sample GCs follow a similar trend, typical for 'young halo' Galactic GCs. We conclude that, as the 'young halo' Galactic GCs, the HB morphologies for the majority of our sample GCs might be, at least partly, influenced by age, in the sense that our sample GCs have redder HBs at a given metallicity.

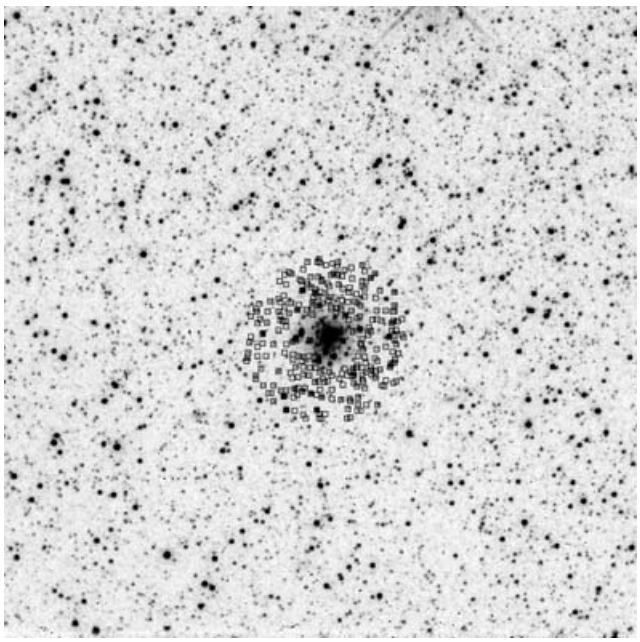

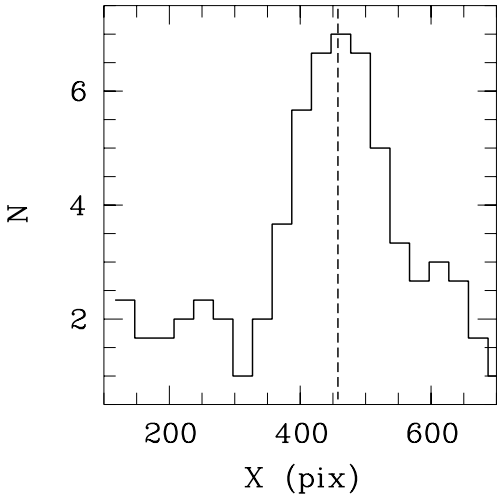

Figure 6. Illustration of our R_{GC} finding technique. Top panel: WFPC2/PC image of FJJI (∼34 × 34 arcsec^2, 750 × 750 pixel). The stars presented in the CMD in Fig. 5 are marked. Bottom panel: distribution of blue stars with $V - I < 0.2$ in a 200 × 800 pixel rectangular area centred on the cluster FJJI. The resulting radius of FJJI is about 100 pixel, which corresponds to 4.6 arcsec.

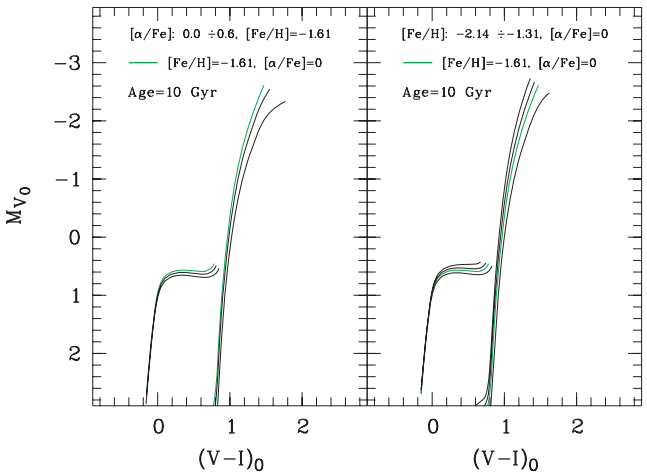

Figure 7. Demonstration of the influence of [α/Fe] and [Fe/H] on the colour of RGB and the luminosity of ZAHB. We show theoretical predictions of the Victoria-Regina stellar models of VandenBerg et al. (2006) for [Fe/H] = −1.6 dex, Age = 10 Gyr and [α/Fe] ratios 0.0, 0.3, 0.6 (left-hand panel) and [Fe/H] = −2.14, −1.84, −1.61, −1.31, Age = 10 Gyr and [α/Fe] = 0 (right-hand panel).

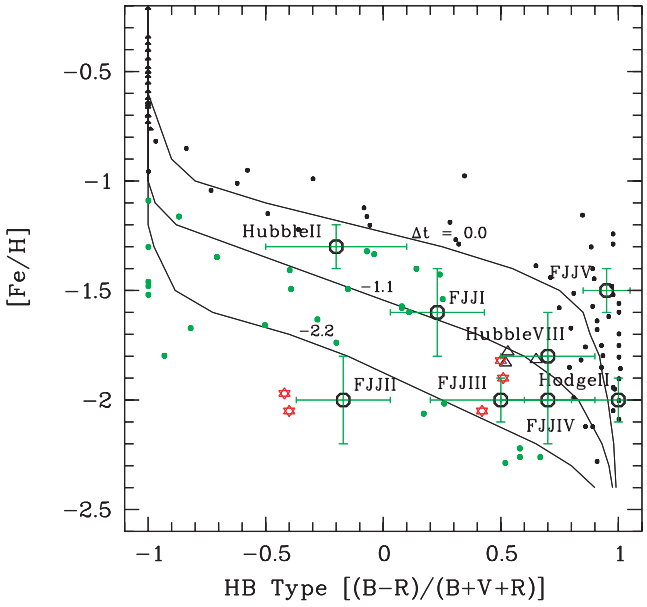

Figure 8. HB-type versus metallicity diagram for our sample GCs (open circles), old halo (dots), disc/bulge (triangles) and young halo Galactic GCs (light filled circles), Fornax dSph (stars) and Sagittarius dSph (open triangles) GC systems. The overplotted isochrones are from Rey et al. (2001). The ages of the isochrones are 0.0, −1.1 and −2.2 Gyr from the top to the bottom.

GCs in nearby dwarf galaxies Sagittarius dSph, Fornax dSph, Magellanic Clouds show similar second-parameter GCs which resemble the 'young halo' Galactic GCs in the HB-type versus [Fe/H] diagram (see e.g. Buonanno et al. 1998, 1999; Strader et al. 2003; Mackey & Gilmore 2004a,b). Rich et al. (2005) studied HB morphologies of 10 GCs in M31 using *HST*/WFPC2 photometry and found metal-poor GCs with HB morphologies resembling those of the Fornax dSph galaxy GCs. It is of interest to continue the CMD studies using high-resolution *HST* imaging for GCs in dwarf galaxies and the outskirts of nearby massive galaxies (e.g. M31) to establish the role of dwarf galaxies and their GC systems as building blocks of massive galaxies in the LG and other nearby groups within 10 Mpc. If most younger halo GCs in massive galaxies were accreted from low-mass satellites, GCs in dwarf galaxies should resemble these younger halo GCs in terms of HB type at a given metallicity. However, we do not know whether these results could be appropriate for probing the formation of more distant galaxies situated in denser environments like Virgo or Fornax clusters.

4.2 Comparison with GCs in M31

Perrett et al. (2002), Beasley et al. (2004, 2005), Fusi Pecci et al. (2005) and Puzia et al. (2005a) studied GCs in the halo of M31 spectroscopically and found that the M31 GCs have essentially distinct

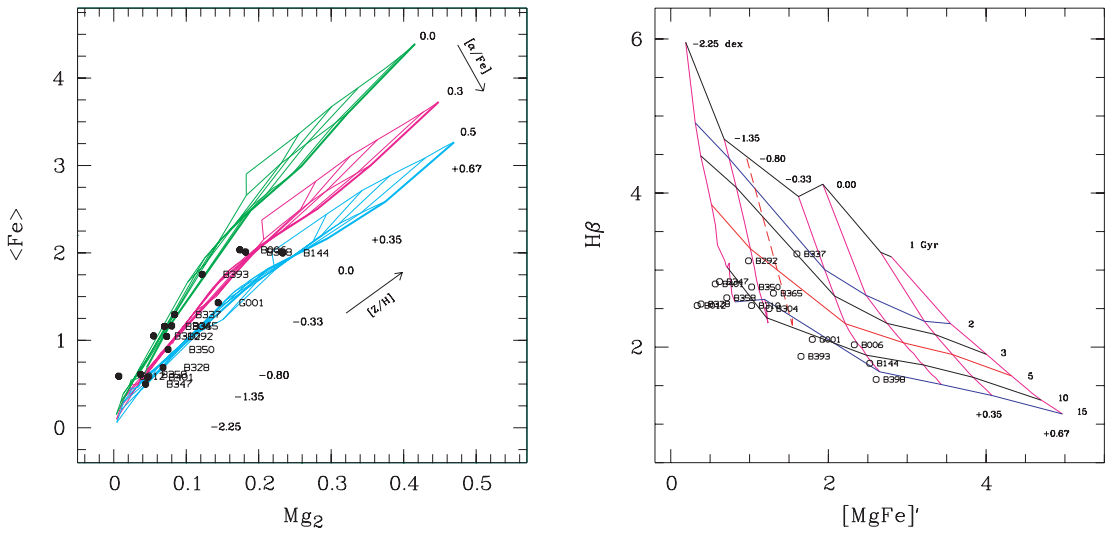

Figure 9. Age–metallicity diagnostic plots for GCs in M31 from a sample of Puzia et al. (2005a). We selected clusters with galactocentric distances greater than ∼40 kpc with the exception of clusters B006 and B012 located near the northern spur (McConnachie et al. 2004) at the projected distances ∼30 kpc and ∼28 kpc from the centre of M31, correspondingly.

properties from those of the MW GCs. The main conclusions from these studies could be summarized as follows. (1) Three types of GC populations exist in the halo of M31: old GCs (>10 Gyr) with a wide range of metallicities, intermediate-age GCs with metallicity [Z/H] ≈ −0.6 and young GCs (⩽1 Gyr) with slightly higher metallicities. (2) The M31 GCs have lower [α/Fe] ratios than the MW GCs (a mean [α/Fe] = 0.14 ± 0.04 dex, Puzia et al. 2005a). (3) The detailed abundances of some elements (e.g. C, N) show a different behaviour with age and metallicity than that of Galactic GCs.

We select halo GCs located at projected galactocentric distances larger than that of NGC 205 (∼40 kpc) from the samples of Worthey (1994), Kuntschner et al. (2002), Beasley et al. (2004) and Puzia et al. (2005a). Fig. 9 shows [α/Fe] and age–metallicity diagnostic plots for these GCs. We expect such clusters to be the most likely candidates for accreted objects resembling ages and chemical compositions similar to GCs in NGC 147, 185 and 205. Indeed, ten of sixteen GCs selected from the sample of Puzia et al. (2005a) are old and metal-poor and are located at similar places in the age–metallicity diagnostic plots as our sample GCs in dwarf galaxies. Only three of them have [α/Fe] ⩽ 0.0 according to the data of Puzia et al. (2005a): B304: ([Z/H] ∼ −1.3, age ∼13 Gyr, [α/Fe] ∼ −0.12), B310: ([Z/H] ∼ −1.6, age ∼12 Gyr, [α/Fe] ∼ −0.33), B358: ([Z/H] ∼ −2.0, age ∼10 Gyr, [α/Fe] ∼ 0.00). Some of the selected M31 GCs show high metallicities and old ages (see right-hand panel of Fig. 9). There are no GCs with such properties in our sample.

One noteworthy case is the M31 GC B337, which is located at a projected distance D_{M31} ∼ 65 kpc from the centre of M31 near the northern stellar spur kinematically associated with NGC 205 (McConnachie et al. 2004). The cluster has an intermediate age of ∼5 Gyr and [Fe/H] ≈ −0.6 dex, and a solar [α/Fe] ratio (Puzia et al. 2005a) similar to that found for Hubble VI in NGC 205 and FJJVII in NGC 185. There are also indication for intermediate-age field stellar populations in the halo of M31 (e.g. Brown et al. 2003, 2006).

Guhathakurta et al. (2006) discovered an extended halo of metal-poor RGB stars out to a projected distance of 165 kpc from the centre of M31. Hence, NGC 147, 185 and 205 with their GCS are embedded in this halo and some clusters may have properties similar to the M31 halo GCs. Pritzl et al. (2005) demonstrated that most Galactic GC stars show similar [α/Fe] ratios as field stars of similar metallicities, and neither clearly resembles the stellar abundances in dwarf galaxies. The situation can be more complex for M31, where the processes of merging and tidal disruption are still active. Additional spectroscopic and CMD studies of GCs in M31 and dwarf satellites are needed to establish the fraction of M31 halo GCs which are twins of the GCs in NGC 147, 185 and 205.

4.3 The diffuse stellar populations

Many authors pointed out the large abundance spread across the RGBs of our sample galaxies. Mould, Kristian & Da Costa (1984) found a mean metallicity for NGC 205 [M/H] $\gtrsim -0.9 \pm 0.2$ and a metallicity dispersion σ [M/H] $\gtrsim$ 0.5 dex. Additionally, these authors obtained a large age spread of RGB stars in the range 2–8 Gyr. Mould, Kristian & Da Costa (1983) estimated a mean metallicity of RGB stars in the outer parts of NGC 147 [M/H] = −1.2 ± 0.2 and a metallicity spread of 0.3 dex. Lee et al. (1993) obtained a metallicity dispersion in NGC 185 in the range −1.6 < [Fe/H] < −0.9 dex from the dispersion of the mean colour of RGB stars measured at M_I = 3.5. Grebel (2000) derived the following values of metallicity and the metallicity spread for NGC 205, 185 and 147 correspondingly: −0.5 ± 0.5, −0.8 ± 0.4 and −1.1 ± 0.4. Mean metallicities estimated by McConnachie et al. (2005) for RGB stars in our sample galaxies are consistent with the data from the aforementioned studies: $[M/H]_{\alpha=0.0}$ = −0.8 for NGC 205, $[M/H]_{\alpha=0.0}$ = −1.2 for NGC185 and $[M/H]_{\alpha=0.0}$ = −1.1 for NGC 147.

High-resolution *HST* images made it possible to study RGB stars closer to the centres of our sample galaxies. Butler & Martinez-Delgado (2005) identified ancient stars in NGC 185 with [Fe/H] $\lesssim$ −1.5 dex with the mean metallicity −1.11 ± 0.08 dex and the last period of active star formation dating about 4 × 10^8 yr ago. The most metal-rich RGB stars in NGC 205 were found to reach [Fe/H] $\gtrsim$ −0.7 dex, while a median value of metallicity for ancient stars in this galaxy is [Fe/H] = −1.06 ± 0.04. Dolphin (2005) using the same observational material and the DOLPHOT program obtained mean metallicities −0.6, −0.9 and −0.9 dex for NGC 205, 185 and 147, respectively.

Our spectroscopic study deals with the integrated light from stars in NGC 205 and 185 very near to the centres of the host galaxies. Hence, it is worth to note that our study supplements the results obtained by the extensive CMD studies. We found $\overline{[Z/H]} \sim 0.5$ dex for the central regions of NGC 205 and a large spread of metallicity ∼0.3–0.4 dex which could not be explained by measurement uncertainties, because the spread is considerably less for GCs having the same S/N in their spectra. We estimate the metallicity of the region of diffuse galactic light in NGC185 near the GC FJJIII ($d_{\rm proj} =$ 0.2 kpc) to be $[Z/H] = -1.16 \pm 0.25$ in a good consent with the CMD studies. As it was also mentioned by Da Costa & Mould (1988) the mean abundance of the associated GCs in each of the studied galaxies is considerably less than that observed for the corresponding field halo stars. So, one could suggest that GCS of these galaxies formed at the earliest epochs of galactic formation along with the first stars.

We found indications for increasing age with increasing galactocentric distance for the field stellar population in NGC 205. The same trend was found in deep CMD studies for stellar populations in NGC 205 and 185. According to Cappellari et al. (1999) there is a central population of stars in NGC 205 with ages in the range 50–100 Myr. AGB stars have solar metallicity and are distributed uniformly over the inner ∼1 arcmin (Davidge 1992). Old stars in NGC 185 form the less concentrated system (Martinez-Delgado, Aparicio & Gallart 1999). The youngest stars are located in the central 150×90-pc^2 region (Butler & Martinez-Delgado 2005). Outside this area only stars with ages $\geqslant$1 Gyr are found.

5 CONCLUSION

Although the modest S/N of some of our GC spectra and the relatively moderate photometric depth of our CMDs do not allow us to derive very accurate ages, we conclude that all our sample GCs appear to be old ($T > 8$ Gyr) and metal-poor ($[Z/H] \lesssim -1.1$), except for the GCs Hubble V in NGC 205 ($T = 1.2 \pm 0.6$ Gyr, $[Z/H] = -0.6 \pm 0.2$), Hubble VI in NGC 205 ($T = 4 \pm 2$ Gyr, $[Z/H] = -0.8 \pm 0.2$) and FJJVII in NGC 185 ($T = 7 \pm 3$ Gyr, $[Z/H] = -0.8 \pm 0.2$). We find two intermediate-age GCs (Hubble VI and FJJVII) which are located at projected distances $D_{\rm proj} \sim 0.3$ and 1.0 kpc from the centres of their host galaxies. Deep images taken with *HST*/ACS are necessary to understand whether these relatively faint star clusters are genuine GCs (i.e. simple stellar populations) born during ∼4–6 Gyr old star formation events in their host galaxies. They could consist also of multiple stellar populations similar to ωCen (see e.g. Sollima et al. 2005).

The HB morphologies for our sample GCs follow the same behaviour with metallicity as younger halo Galactic GCs. It was found for Galactic GC, that age may not be the dominant second parameter determining the shape of the HBs of the GCs (see e.g. Stetson, Vandenberg & Bolte 1996). GCs having blue HBs are in general older than 10 Gyr (Lee et al. 1994). So, we suggest here that the HB morphologies for our sample GCs likely do not bias our spectroscopic age estimates based on Balmer absorption-line indices.

We find that most of the GCs in the studied galaxies are weakly or not α-enhanced, in contrast to the population of GCs in nearby early-type galaxies (see Puzia, Kissler-Patig & Goudfrooij 2006). The chemical composition of GCs may turn out to be a powerful tool to discriminate between clusters which formed *in situ* in massive galaxies and those that were formed in smaller subunits and later accreted in more massive haloes.

Spectroscopic ages and metallicities of the central regions in NGC 205 and 185 coincide with those obtained from CMDs. The central field stellar populations in these galaxies have approximately the same age as their most central GCs Hubble V in NGC 205 and FJJIII in NGC 185, respectively, but are more metal-rich than the central GCs.

ACKNOWLEDGMENTS

MES acknowledges all participants of the project SCORPIO at scientific advisory of Professor V. L. Afanasiev for their extensive work on designing, producing and testing the SCORPIO spectrograph with the multislit unit at the 6-m telescope. THP is supported by an ESA Research Fellowship, which is gratefully acknowledged. THP also acknowledges partial financial support through grant GO-10129 from the Space Telescope Science Institute, which is operated by AURA, Inc., under NASA Contract NAS5-26555. MES thanks Don VandenBerg for his help in applying his models to the analysis of the CMDs for GCs in NGC 205, N. A. Tiknonov, D. I. Makarov, O. K. Sil'chenko, O. A. Galazutdinova, G. M. Beskin. We thank the anonymous referee for valuable comments. VLA acknowledges the INTAS grant (96-0315), the 'Astronomy' Federal Science and Technology Program (contract no. 40.022.1.1.1101 from 2002 February 1) and the Programme of the Department of Physical Sciences of the Russian Academy of Sciences for partial support of his work. The 6-m telescope of the Special Astrophysical Observatory of the Russian Academy of Sciences is operated under the financial support of the Science Department of Russia (registration no. 01-43). Some of the data presented in this paper were obtained from the Multimission Archive at the Space Telescope Science Institute (MAST). STScI is operated by the Association of Universities for Research in Astronomy, Inc., under NASA contract NAS5-26555. Support for MAST for non-*HST* data is provided by the NASA Office of Space Science via grant NAG5-7584 and by other grants and contracts. This research has made use of NASA's Astrophysics Data System Bibliographic Services.

REFERENCES

Afanasiev V. L., Moiseev A. V., 2005, Astron. Lett., 31, 194
Barmby P., Huchra J. P., 2001, AJ, 122, 2468
Beasley M. A., Brodie J. P., Strader J., Forbes D. A., Proctor R. N., Barmby P., Huchra J. P., 2004, AJ, 128, 1623
Beasley M. A., Brodie J. P., Strader J., Forbes D. A., Proctor R. N., Barmby P., Huchra J. P., 2005, AJ, 129, 1412
Bender R., Paquet A., Nieto J.-L., 1991, A&A, 246, 349
Bonifacio P., Hill V., Molaro P., Pasquini L., Di Marcantonio P., Santin P., 2000, A&A, 359, 663
Brown T. M., Ferguson H. C., Smith E., Kimble R. A., Sweigart A. V., Renzini A., Rich R. M., VandenBerg D. A., 2003, ApJ, 592, L17
Brown T. M., Smith E., Guhathakurta P., Rich R. M., Ferguson H. C., Renzini A., Sweigart A. V., Kimble R. A., 2006, ApJ, 636, L89
Buonanno R., Corsi C. E., Zinn R., Fusi Pecci F., Hardy E., Suntzeff N. B., 1998, ApJ, 501, L33
Buonanno R., Corsi C. E., Castellani M., Marconi G., Fusi Pecci F., Zinn R., 1999, AJ, 118, 1671
Butler D. J., Martinez-Delgado D., 2005, AJ, 129, 2217
Burstein D., Faber S. M., Gaskell C. M., Krumm N., 1984, ApJ, 287, 586
Brusual G., Charlot S., 2003, MNRAS, 344, 1000
Carter D., Sadler E. M., 1990, MNRAS, 245, 12
Cappellari M., Bertola F., Burstein D., Buson L. M., Greggio L., Renzini A., 1999, ApJ, 515, L17
Chilingarian I., Prugniel P., Sil'chenko O., Afanasiev V., 2005, in Jerjen H., Binggeli B., eds, IAU Colloqium No. 198, Near-field Cosmology with Dwarf Elliptical Galaxies. Cambridge Univ. Press, Cambridge, p. 105
Covino S., Galletti S., Pasinetti L. E., 1995, A&A, 303, 79

Da Costa G. S., Mould J. R., 1988, ApJ, 334, 159
Davidge T. J., 1992, ApJ, 397, 457
Davidge T. J., 1994, AJ, 108, 2123
Davidge T. J., 2005, AJ, 130, 2087
Dolphin A. E., 2000a, PASP, 112, 1383
Dolphin A. E., 2000b, PASP, 112, 1397
Dolphin A. E., Saha A., Skillman E. D., Dohm-Palmer R. C., Tolstoy E., Cole A. A., Gallagher J. S., Hoessel J. G., 2003, AJ, 126, 187
Dolphin A. E., 2005, in Valls-Gabaud D., Chavez M., eds, ASP Conf. Ser. Vol. TBA, Resolved Stellar Populations. Astron. Soc. Pac., San Francisco, p. 74
Ford H. C., Jacoby G., Jenner D. C., 1977, ApJ, 213, 18
Fusi Pecci F., Bellazzini M., Buzzoni A., De Simone E., Federici L., 2005, AJ, 130, 554
Gallagher J. S., Grebel E. K., 2001, in Geisler D., Grebel E., Minniti D., eds, IAU Symp. 207, Extragalactic Star Clusters. Astron. Soc. Pac., San Francisco, p. 745
Galleti S., Federici L., Bellazzini M., Fusi Pecci F., Macrina S., 2004, A&A, 416, 917
Galleti S., Federici L., Bellazzini M., Buzzoni A., Fusi Pecci F., 2006, preprint (astro-ph/0605718)
Geisler D., 1999, in Whitelock P., Cannon R. D., eds, IAU Symp. 192, Stellar Content of the Local Group. Astron. Soc. Pac., San Francisco, p. 231
Geisler D., Smith V. V., Wallerstein G., Gonzalez G., Charbonnel C., 2005, AJ, 129, 1428
Grebel E. K., 2000, in Favata F., Kaas A. A., Wilson A., eds, 33rd ESLAB Symp., Star Formation from the Small to the Large Scale. ESA Publications Division, Noordwijk, SP-445, p. 87
Guhathakurta P., Ostheimer J. O., Gilbert K. M., Rich R. M., Majewski S. R., Kalirai J. S., Reitzel D. B., Patterson R. J., 2005, preprint (astro-ph/0605172)
Harbeck D. et al., 2001, AJ, 122, 3092
Harris W. E., 1996, AJ, 112, 1487, for the 2003 update see http://physun.physics.mcmaster.ca/~harris/mwgc.dat
Hodge P. W., 1973, ApJ, 182, 671
Hodge P. W., 1974, PASP, 86, 289
Hodge P. W., 1976, AJ, 81, 25
Hubble E., 1932, ApJ, 76, 44
Huxor A. P., Tanvir N. R., Irwin M. J., Ibata R., Collett J. L., Ferguson A. M. N., Bridges T., Lewis G. F., 2005, MNRAS, 360, 1007
Hwang N. et al., 2005, in Jerjen H., Binggeli B., eds, IAU Colloqium No. 198, Near-field Cosmology with Dwarf Elliptical Galaxies. Cambridge Univ. Press, Cambridge, p. 257
Jones D. H. et al., 1996, ApJ, 466, 742
Kuntschner H., Ziegler B. L., Sharples R. M., Worthey G., Fricke K. J., 2002, A&A, 395, 791
Lanfranchi G. A., Matteucci F., 2003, MNRAS, 345, 71
Lee M. G., 1996, AJ, 112, 1483
Lee M. G., Freedman W. L., Madore B. F., 1993, AJ, 106, 964
Lee Y.-W., Demarque P., Zinn R., 1994, AJ, 423, 248
Mackey A. D., Gilmore G. F., 2004a, MNRAS, 352, 153
Mackey A. D., Gilmore G. F., 2004b, MNRAS, 355, 504
Martinez-Delgado D., Aparicio A., Gallart C., 1999, AJ, 118, 2229
Mateo M., 1998, ARA&A, 36, 435
McConnachie A. W., Irwin M. J., Lewis G. F., Ibata R. A., Chapman S. C., Ferguson A. M. N., Tanvir N., 2004, MNRAS, 351, L94
McConnachie A. W., Irwin M. J., Ferguson A. M. N., Ibata R. A., Lewis G. F., Tanvir N., 2005, MNRAS, 356, 979
Mould J., Kristian J., Da Costa G. S., 1983, ApJ, 270, 471
Mould J., Kristian J., Da Costa G. S., 1984, ApJ, 278, 575
Perrett K. M., Bridges T. J., Hanes D. A., Irwin M. J., Brodie J. P., Carter D., Huchra J. P., Watson F. G., 2002, AJ, 123, 2490
Pipino A., Matteucci F., Chiappini C., 2006, AJ, 638, 739
Pritzl B. J., Venn K. A., Irwin M., 2005, AJ, 130, 2140
Proctor R. N., Forbes D. A., Beasley M. A., 2004, MNRAS, 355, 1327
Puzia T. H., Saglia R. P., Kissler-Patig M., Maraston C., Greggio L., Renzini A., Ortolani S., 2002, A&A, 395, 45
Puzia T. H. et al., 2004, A&A, 415, 123
Puzia T. H., Perrett K. M., Bridges T. J., 2005a, A&A, 434, 909
Puzia T. H. et al., 2005b, A&A, 439, 997
Puzia T. H., Kissler-Patig M., Goudfrooij P., 2006, ApJ, 648, 383
Rey S.-C., Yoon S.-J., Lee Y.-W., Chaboyer B., Sarajedini A., 2001, AJ, 122, 3219
Rich M., Corsi C. E., Cacciari C., Federici L., Fusi Pecci F., Djorgovski S. G., Freedman W. L., 2005, AJ, 129, 2670
Salaris M., Weiss A., 2002, A&A, 388, 492
Saviane I., Held E. V., Bertelli G., 2000, A&A, 355, 56
Schlegel D. J., Finkbeiner D. P., Davis M., 1998, ApJ, 500, 525
Sharina M. E., Afanasiev V. L., Puzia T. H., 2006, Astrophys. Lett., 32, 185
Sharov A. C., Lyuty V. M., 1983, Ap&SS, 90, 371
Shetrone M. D., Bolte M., Stetson P. B., 1998, AJ, 115, 1888
Shetrone M. D., Cote P., Sargent W. L. W., 2001, ApJ, 548, 592
Shetrone M., Venn K. A., Tolstoy E., Primas F., Hill V., Kaufer A., 2003, AJ, 125, 684
Simien F., Prugniel Ph., 2002, A&A, 384, 371
Smecker-Hane T., McWilliam A., 1999, in Hubeny I., Heap S., Cornett R., eds, ASP Conf. Ser. Vol. 192, Spectrophotometric Dating of Stars and Galaxies. Astron. Soc. Pac., San Francisco, p. 150
Sollima A., Pancino E., Ferraro F. R., Bellazzini M., Straniero O., Pasquini L., 2005, ApJ, 634, 332
Stetson P. B., Vandenberg D. A., Bolte M., 1996, PASP, 108, 560
Strader J., Brodie J. P., Forbes D. A., Beasley M. A., Huchra J. P., 2003, AJ, 125, 1291
Stuard A., Ord J. K., 1994, Kendalls Advanced Theory of Statistics Vol. 1; Distribution Theory, 6th edn. Edward Arnold, London
Thomas D., Maraston C., Bender R., 2003, MNRAS, 339, 897
Thomas D., Maraston C., Korn A., 2004, MNRAS, 351, L19
Tolstoy E., Venn K. A., Shetrone M., Primas F., Hill V., Kaufer A., Szeifert T., 2003, AJ, 125, 707
Tonry J., Davis M., 1979, AJ, 84, 1511
Trager S. C., Worthey G., Faber S. M., Burstein D., Gonzalez J. J., 1998, ApJS, 116, 1
van den Bergh S., 1969, ApJS, 19, 145
van den Bergh S., 2000, The Galaxies of the Local Group. Cambridge Univ. Press, Cambridge
VandenBerg D. A., Bergbusch P. A., Dowler P. D., 2006, ApJS, 162, 375
Vazdekis A., 1999, ApJ, 513, 224
Worthey G., 1994, ApJS, 95, 107
Worthey G., Ottaviani D. L., 1997, ApJS, 111, 377
Worthey G., Faber S. M., Gonzalez J. J., Burstein D., 1994, ApJS, 94, 687
Young L. M., Lo K. Y., 1997, AJ, 476, 127
Zinn R., 1993, in Smith G. H., Brodie J. P., eds, The Globular Cluster–Galaxy Connection. Astron. Soc. Pac., San Francisco, p. 38

This paper has been typeset from a TEX/LATEX file prepared by the author.